The age and origin of cratonic lithospheric mantle: Archean dunites vs. Paleoproterozoic harzburgites from the Udachnaya kimberlite, Siberian craton

Dmitri Ionov, Zhe Liu, Jie Li, Alexander Golovin, Andrey Korsakov, Yigang Xu

The age and origin of cratonic lithospheric mantle: Archean dunites vs. Paleoproterozoic harzburgites from the Udachnaya kimberlite, Siberian craton

Dmitri A. Ionov[a,b*], Zhe Liu[a], Jie Li[a], Alexander V. Golovin[c], Andrey V. Korsakov[c], Yigang Xu[a]

[a] *State Key Laboratory of Isotope Geochemistry, Guangzhou Institute of Geochemistry, Chinese Academy of Sciences, 510640 Guangzhou, China*

[b] *Géosciences Montpellier, University of Montpellier, 34095 Montpellier, France*

[c] *V.S. Sobolev Institute of Geology and Mineralogy, Siberian Branch, Russian Academy of Sciences and Novosibirsk State University, Novosibirsk 630090, Russia*

∗ *Corresponding author; e-mail: dionov@umontpellier.fr, phone: +33 (0)467143349*

11996 words in the main text

ABSTRACT *(485words)*

Cratonic lithospheric mantle is believed to have been formed in the Archean, but kimberlite-hosted coarse peridotites from Udachnaya in the central Siberian craton typically yield Paleoproterozoic Re-depletion Os isotope ages (T_{RD}). By comparison, olivine megacrysts from Udachnaya, sometimes called "megacrystalline peridotites", often yield Archean T_{RD} ages, but the nature of these rare materials remains enigmatic. We provide whole-rock (WR) Re-Os isotope and PGE analyses for 24 olivine-rich xenoliths from Udachnaya as well as modal and petrographic data, WR and mineral major and trace element compositions. The samples were selected based on (a) high olivine abundances in hand specimens and (b) sufficient freshness and size to yield representative WR powders. They comprise medium- to coarse-grained (olivine <1 cm) dunites, a megacrystalline (olivine >1 cm) dunite, olivine megacrysts and low-orthopyroxene (11–21% opx) harzburgites equilibrated at 783–1154°C and 3.9–6.5 GPa; coarse dunites have not been previously reported from Udachnaya; two xenoliths contain ilmenite. The harzburgites and dunites have similar WR variation ranges of Ca, Al, Fe, Cr and Mg# (0.917–0.934) typical of refractory cratonic peridotites, but the dunites tend to have higher MgO, NiO and Mg/Si. Mineral abundances and those of Ca and Al are not correlated with $Mg\#_{WR}$; they are not due to differences in melting degrees but are linked to metasomatism. Several samples with high $^{187}Re/^{188}Os$ show a positive linear correlation with $^{187}Os/^{188}Os$ with an apparent age of 0.37 Ga, same as eruption age of host kimberlite. Robust T_{RD} ages were obtained for 16 xenoliths with low $^{187}Re/^{188}Os$ (0.02–0.13). T_{RD} ages for low-opx harzburgites (1.9–2.1 Ga; average 2.0 ± 0.1 Ga) are manifestly lower than for dunites and megacrysts (2.4–3.1 Ga); the latter define two subsets with average T_{RD} of 2.6 ± 0.1 Ga and 3.0 ± 0.1 Ga, and T_{MA} of 3.0 ± 0.2 Ga and 3.3 ± 0.1 Ga, respectively. Differences in olivine grain size (coarse vs. megacrystalline) are not related to age. The age relations suggest that the dunites and megacrysts could not be produced by re-melting of

harzburgites, e.g. in arc settings, nor be melt channel materials in harzburgites. Instead, they are relict fragments of lithospheric mantle formed in the Archean (likely in two events at or after 2.6 Ga and 3.0 Ga) that were incorporated into cratonic lithosphere during the final assembly of the Siberian craton in the Paleoproterozoic. A multi-stage formation of the Siberian lithospheric mantle is consistent with crustal basement ages from U-Pb dating of zircons from crustal xenoliths at Udachnaya and detrital zircons from the northern Siberian craton (1.8–2.0, 2.4–2.8 and 3.0–3.4 Ga). The new data from the Siberian and other cratons suggest that the formation of strongly melt-depleted cratonic lithosphere (e.g. Mg# ≥0.92) did not stop at the Archean-Proterozoic boundary as is commonly thought, but continued in the Paleoproterozoic. The same may be valid for the transition from the 'Archean' (4–2.5 Ga) to modern tectonic regimes.

KEYWORDS: lithospheric mantle; Siberian craton; dunite; harzburgite; Re-Os isotopes; highly siderophile elements

1. Introduction

1.1. *Formation stages of the Siberian craton*

Cratons are the oldest parts of continents. Essential components of their crustal basement are Archean (>2.5 Ga) magmatic and metamorphic rocks with widespread ~2.7 Ga and older ages (e.g. Condie, 2014). The only robust dating methodology for refractory peridotites, the main components of cratonic mantle, is based on the Re-Os isotope system because Os is highly compatible during mantle melting. These rocks do not normally show isochrone relations (e.g. Rudnick and Walker, 2009), but their formation can be traced back using model "Re-depletion" ages (T_{RD}) assuming that all Re was extracted from pristine mantle in a single, high-degree (≥30%) melting event (Walker et al., 1989). The T_{RD} method was defined for whole-rock (WR) peridotite xenoliths, and initially applied to analytical samples from the Kaapvaal and Siberian cratons prepared from large amounts (hundreds of grams) of material required to bridge modal heterogeneities in coarse-grained rocks and thus provide representative compositional data (Boyd et al., 1997; Pearson et al., 1995b; Walker et al., 1989). The T_{RD} values for individual samples have high uncertainties, and it is common to constrain lithospheric formation ages based on either peaks on T_{RD} frequency distribution plots or the oldest ages whereas dispersed younger T_{RD} values are more likely to be due to more recent melt metasomatism (e.g. Carlson et al., 1999; Irvine et al., 2003).

Rhenium-osmium isotope data on coarse (low-T) WR peridotites show that the lithospheric mantle beneath several well-studied cratons in North America and South Africa formed in the Archean, with T_{RD} distribution peaks at 2.6 to 2.8 Ga (e.g. Carlson et al., 2005; Wittig et al., 2010b). The similar crust and mantle formation ages (crust-mantle coupling, (e.g. Pearson et al., 1995a)) are two related facets of lithosphere development, i.e. melt extraction from fertile mantle yields both refractory residues that form lithospheric mantle and mafic melts that form cratonic proto-crust (Herzberg and Rudnick, 2012; Moyen et al., 2017).

The formation (melt extraction) age for the lithospheric mantle of the Siberian craton, however, continues to be debated. Peridotite xenoliths suitable for Re-Os dating are available almost exclusively from two kimberlite pipes: Udachnaya in the center of the craton and Obnazhennaya near its northeastern (NE) margin (KML file). Published T_{RD} estimates for WR refractory peridotites from both pipes are puzzling because they show bimodal distribution with peaks at ~2.0 Ga and 2.8 Ga (Ionov et al., 2015a). The pioneering work of Pearson et al. (1995b) provided T_{RD} values for 16 olivine-rich xenoliths from Udachnaya including four Archean (2.6–3.2 Ga) and eight Paleoproterozoic (1.7–2.2 Ga) ages, as well as four younger (0.9–1.4 Ga) values attributed to metasomatism. Pearson et al. (1995b) argued for an Archean (≥3.2 Ga) formation age for the Siberian craton mantle and downplayed the Paleoproterozoic T_{RD} values, in spite of their greater numbers. For instance, they speculated that the Archean materials may be located deeper in the lithosphere than the Paleoproterozoic peridotites.

Later work, by contrast, found mainly Paleoproterozoic ages for a range of mantle samples from Udachnaya. Ionov et al. (2015b) reported Re-Os isotope data for 29 WR peridotites and obtained ~2 Ga T_{RD} values for the majority of coarse refractory rocks (Mg# 0.92–0.93), which they viewed as pristine melting residues, as well as generally lower (0.9–2.0 Ga) estimates for deformed, low-Mg# (0.907–0.919) garnet peridotites they ascribed to the effects of melt metasomatism on 2 Ga old residues. Doucet et al. (2015) obtained ~1.8 Ga model Hf-Nd isotope ages for spinel harzburgites from the same suite while Wiggers de Vries et al. (2013) reported ~1.8 Ga T_{RD} ages for sulfide inclusions in diamonds. Peridotite xenoliths from the Obnazhennaya kimberlite, by comparison, show both Archean and Paleoproterozoic ages (peaks at 2.8 and 1.9 Ga), with no relation to their modal (dunites or harzburgites) or WR major element compositions (Ionov et al., 2015a). Likewise, Moyen et al. (2017) reported a bimodal age distribution for crustal xenoliths from Udachnaya (~1.9 Ga for the lower crust

and ~2.8 and for the upper crust) and suggested that the Siberian cratonic lithosphere formed in two stages, i.e. first in the Archean, then in the Paleoproterozoic when much of the pre-existing lithospheric mantle and lower crust was replaced with younger melting residues.

An alternative approach to dating Udachnaya peridotites was employed by Pernet-Fisher et al. (2015) who reported Re-Os isotope data not on representative WR samples, but on small amounts of material extracted from five xenoliths and on olivine separates from another five xenoliths. The advantages of such an approach are that small xenoliths are easier to find and handle, yet, the absence of modal and WR chemical data, that are essential to assess the melting and metasomatism history of the mantle, adds uncertainties to age estimates and their interpretation. Pernet-Fisher et al. (2015) obtained T_{RD} values from ≤0 to 2.7 Ga and argued that they record melt extraction events ranging from ~3 Ga to ~1.2 Ga despite strong evidence (common deformation, low olivine Mg# (0.894–0.914) and high Re/Os ratios) for melt metasomatism evoked for such samples in earlier studies of Udachnaya xenoliths (Agashev et al., 2013; Ionov et al., 2015b; Pearson et al., 1995b). Finally, Pernet-Fisher et al. (2019) reported Archean T_{RD} values for fragments of seven (out of eleven analysed) olivine megacrysts from Udachnaya (apparently similar to those analysed by Pearson et al. (1995b)).

To sum up, three formation models have been proposed for the mantle lithosphere of the Siberian craton: (1) overall Archean (≥3 Ga) formation age (Pearson et al., 1995b; Pernet-Fisher et al., 2019), (2) continuous or multi-stage formation from the Eoarchean to Mesoproterozoic (Pernet-Fisher et al., 2015), and (3) a two-stage formation based on bimodal age distribution for mantle and crustal rocks (Ionov et al., 2015b; Moyen et al., 2017).

1.2. *The enigmatic nature of the oldest materials in the Siberian cratonic mantle*

The nature of the rare mantle materials with Archean ages from Udachnaya remains enigmatic. Textural, modal, chemical and isotopic features of such xenoliths, and their

differences with younger rocks, must be constrained to gain insights into the earliest stages of lithospheric formation in the central Siberian craton. Pearson et al. (1995b) referred to three out of four of their Archean samples as "megacrystalline peridotites", for which only qualitative descriptions and mineral analyses were reported. Their $Mg\#_{ol}$ [$Mg/(Mg+Fe)_{at}$ of olivine] (0.922–0.927) fall in the range for coarse harzburgites from Udachnaya (0.919–0.930) with ~2 Ga T_{RD} ages (Doucet et al., 2013; Ionov et al., 2015b); some contain rare sub-calcic garnets (Pokhilenko et al., 1991; Sobolev et al., 1984), but published data are too scarce to assess links of Archean ages with garnet compositions. Another Archean sample, spinel peridotite UV191/89 (Pearson et al., 1995b) was reported to contain 12% orthopyroxene (opx), but is referred to as dunite (Boyd et al., 1997).

Pearson et al. (1995b) linked the Archean ages chiefly to "megacrystalline peridotites" (probably, olivine megacrysts), but the absence of petrographic descriptions and quantitative data on modal or bulk chemical compositions of these samples renders it difficult to constrain their origin and compare them to other mantle xenoliths. Sobolev et al. (1984) collected ~300 olivine megacrysts and what they call "megacrystalline dunites" at Udachnaya. Most of them are very small (1–3 cm), with few samples >5 cm in at least one dimension; the largest olivine grains measure ~10 cm, but their size varies both within and between the samples, and grades to <1 cm. The megacrystalline olivine may contain inclusions of garnet (mainly Ca-poor, Cr-rich), less commonly, Cr-spinel, opx, clinopyroxene (cpx) and ilmenite, i.e. minerals also common in coarse peridotites. Pernet-Fisher et al. (2019) used He-Os isotope and trace element data for olivine megacrysts from Udachnaya to examine their metasomatism but did not address the origin of these exotic materials (especially, how they could be produced by melt extraction) or their relations with coarse harzburgites.

A particular problem is ambiguous terminology and sample descriptions in the previous studies. Pernet-Fisher et al. (2019) described each of their samples as "one large megacryst"

of olivine (mainly ≤2–3 cm in size), yet also called them "megacrystalline dunites", a term appropriate for rocks composed of aggregates of olivine grains, but questionable for single olivine crystals. For instance, kimberlites at Udachnaya and elsewhere commonly contain large mantle-derived clinopyroxene crystals (Abersteiner et al., 2019), but they are not referred to as "megacrystalline pyroxenites". "Megacrystalline dunites" analyzed by Pearson et al. (1995b) may rather be olivine megacrysts as well, i.e. essentially the same kind of materials as those reported later by Pernet-Fisher et al. (2019).

Overall, it is not clear what distinguishes these Archean materials from post-Archean spinel and garnet peridotites from Udachnaya: their ultra-coarse grain size, their high modal olivine or other parameters. It appears that Archean T_{RD} ages for Udachnaya have been so far obtained almost exclusively on olivine megacrysts. This also raises a question whether the Udachnaya-East kimberlites enclose any normal dunites, i.e. poly-grain olivine-rich rocks similar in grain size to other peridotite xenoliths, like dunites in the Obnazhennaya kimberlite (Ionov et al., 2015a).

1.3. *Objectives of this study*

Given the limited number of samples studied and the dearth of petrologic and chemical WR data reported (Pearson et al., 1995b; Pernet-Fisher et al., 2019), the nature of Archean mantle materials from Udachnaya, in particular of the megacrystalline xenoliths and coarse olivine-rich peridotites, remains to be fully established. To address the unresolved questions, we collected and studied olivine-rich Udachnaya peridotites regardless of their grain size, sufficiently large to yield representative WR powders. Robust modal, WR chemical data and formation ages for these potentially oldest lithospheric mantle materials in Siberia, including ultra-coarse-grained xenoliths, are essential to constraining their origin, notably melting history in relation to relevant experimental data (e.g. Herzberg, 2004; Walter, 2003).

Here we provide the first comprehensive set of petrologic, geochemical and age data for main types of the most refractory xenolith materials in kimberlites from the Siberian craton: dunites (including their "megacrystalline" variety) and olivine-rich harzburgites, as well as large olivine megacrysts reported in earlier studies (Pearson et al., 1995b; Pernet-Fisher et al., 2019). We report highly siderophile element (HSE) concentration data and Os isotopic compositions for 24 new, olivine-rich peridotites, as well as three opx-rich xenoliths, from the Udachnaya kimberlite together with modal and petrographic data, bulk-rock and mineral major and trace element compositions. The major objectives of this paper are to: (a) establish the Os isotope and HSE distribution in these materials; (b) better constrain their formation (melt extraction) ages, and (c) examine relations between the mantle and crustal components of different ages during the formation and assembly of the central Siberian craton.

2. Geological setting and samples

2.1. *Geologic setting of the Udachnaya pipe*

The Udachnaya kimberlite (66°26'N, 112°19'E) is located in the Sakha (Yakutia) Republic of the Russian Federation, close to the center of Siberia (KML file). It belongs to the Daldyn-Alakit field in the southwestern portion of the Yakutian kimberlite province that extends from the center to northern and NE parts of the Siberian craton (KML file). The kimberlite was mined for diamonds in an open pit in 1971–2015. From 2015, the mining and crushing have been done underground making it unlikely for more xenoliths to be recovered. Samples in this study were collected at ~400–640 m depth near the center of the Udachnaya-East pipe in remarkably well-preserved type-I kimberlite (Kamenetsky et al., 2012) or in the storage area of mined materials from the same depth range. They are generally less altered than samples found near the surface or at shallow levels in the mine (e.g. Boyd et al., 1997; Pearson et al., 1995b).

The pipe is hosted by Neoproterozoic to Paleozoic sedimentary rocks, and is believed to be located in the Daldyn block of the craton. This block is exposed on the Anabar shield north of Udachnaya, where crustal rocks have U-Pb zircon ages from 1.8 to 3.4 Ga with three main periods: 1.8–2.0 Ga, 2.4–2.8 Ga and 3.0–3.4 Ga (Paquette et al., 2017). U-Pb dating of perovskite in kimberlite yielded an eruption age of 367±5 Ma for the Udachnaya-East pipe and a range from 353±5 to 361±4 Ma for the adjacent Udachnaya-West as well as several other pipes in the Daldyn field (Kinny et al., 1997). Other estimates range from 347 to 429 Ma (see Ionov et al. (2015b)). For simplicity, and in line with some previous peridotite xenolith studies (e.g. Ionov et al., 2015b), we assume below an eruption age of 360 Ma.

Previous work has provided much information about the Udachnaya kimberlite and its various xenolithic materials (Abersteiner et al., 2018; Agashev et al., 2013; Golovin et al., 2018; Jean et al., 2016; Kamenetsky et al., 2014; Kamenetsky et al., 2012; Kamenetsky et al., 2008; Kitayama et al., 2017; Pernet-Fisher et al., 2019; Sobolev et al., 2009; Spetsius and Serenko, 1990). Multi-discipline studies of a suite of large, fresh peridotite xenoliths from Udachnaya have provided comprehensive data on their petrography and chemical composition (Doucet et al., 2013; Doucet et al., 2012; Doucet et al., 2014; Goncharov et al., 2012; Ionov et al., 2010), radiogenic and stable isotopes (Doucet et al., 2016; Ionov et al., 2017; Kang et al., 2017; Xia et al., 2017) as well as petrophysical properties (Bascou et al., 2011) that address melt extraction and metasomatism during the formation and evolution of the cratonic lithosphere.

2.2. *Sample selection and preparation*

Olivine-rich xenoliths, including olivine megacrysts and "megacrystalline dunites" ≥5 cm in size were targeted in the field in recent years, but they are very scarce and usually hard to recover from massive kimberlites in Udachnaya. In addition, hundreds of xenoliths collected

by AVG and AVK since 2003 were re-examined to select olivine-rich (≥80%) samples, regardless of their grain size. Twenty-four such xenoliths (including U220 earlier reported by Ionov et al. (2010)) were chosen for this study based on their size, low alteration degrees and high modal olivine (from visual inspection) without preference for any rock type. Three opx-rich rocks were included as well for comparison. The samples are listed in Table 1, which provides a summary of essential data for each xenolith; the full dataset is given in Electronic Supplement 1 (ES1).

The xenoliths ranged in size from 5 to 20 cm. It may not be certain if some very coarse-grained samples 5–10 cm in size are large enough to prepare representative WR powders, but they appear to be the largest samples currently available for these rare rock types, and no larger xenoliths from Udachnaya may be accessible in the future. Their rinds were removed by hammer or by sawing if they contained kimberlite or alteration products; sawn surfaces were cleaned on alumina disks. Material from xenolith cores (32–250 g and an ilmenite-bearing sample of 16 g; Table 1) was inspected to make sure it contained no veins or modal gradations and crushed to <5–10 mm in a jaw crusher with ceramic jaws and inner walls. Photographs of WR samples prepared for crushing are given in Electronic Supplement 2 (ES2). Splits of crushed material (10–20 g) were ground to fine powder in agate. The crusher and jars (see photos in ES2) were carefully cleaned to avoid cross-contamination.

3. Methods

Detailed descriptions of the methods are provided in ES3.

3.1. *Major elements, modal compositions and P-T estimates*

Whole rock major element compositions were obtained by wavelength-dispersive (WD) X-ray fluorescence (XRF) spectrometry at J. Gutenberg University, Mainz. Rock powders were ignited for ≥3 h at 1000°C to turn all FeO into Fe_2O_3, expel volatiles, and measure the loss on

ignition (LOI). Glass beads, produced by fusing 0.8 g of ignited powders with 4.8 g of dried LiB_4O_7 (1:7 dilution) were analyzed on a Philips PW 1404 spectrometer using ultramafic and mafic reference samples as external standards. Peridotite reference samples JP-1 and UBN were analyzed as unknowns to control accuracy with results close to recommended values (ES1). The compositions are reported with Fe_2O_3 recalculated to FeO.

Minerals were analyzed for major elements by WD electron probe microanalysis (EPMA) at the Guangzhou Institute of Geochemistry, Chinese Academy of Sciences (GIG-CAS) in grain mounts. Garnet and spinel were run on a JXA-8900 instrument at 20 kV accelerating voltage, 40 nA beam current, 1–3 mm beam diameter, counting times of 20–40 s for peaks and 20–40 s for background (Ziberna et al., 2016) with ZAF data reduction procedure. Olivine and pyroxenes (homogeneous cores delimited using BSE imaging) were analyzed on Cameca SXFive FE. Olivine was run at 20 kV, 20–60 s peak counting time, and the current of 20 nA and 100 nA. Data obtained at 20nA are reported for Si, Fe, Mn and Ni, and data at 100 nA for Cr, Ca and Na; concentrations of Al and Ti are below detection for nearly all samples. Machine drift and accuracy were monitored with the MongOl reference sample (Batanova et al., 2019), see ES3. Pyroxenes were run at 20 kV, 40 nA, 1–3 mm beam, and 40 s counting times for peaks and background; the PAP procedure was used for matrix correction.

Equilibration temperatures (T) were calculated based on the following mineral pairs and methods depending on the minerals present: (a) cpx-opx (Taylor, 1998); (b) Ca-in-cpx (Nimis and Taylor, 2000); (c) Ca-in-opx (Brey and Köhler, 1990) corrected as in Nimis and Grütter (2010); (d) opx-garnet (Nimis and Grütter, 2010). Equilibration pressure was estimated with opx-garnet barometer of Nickel and Green (1985); for spinel peridotites it was evaluated based on projection of their equilibration T's to local geotherm (Goncharov et al., 2012), and for garnet peridotites using P values for samples with similar T's.

Modal abundances were calculated from a least-squares fit of the WR major element

285 composition to its constituent minerals. The method chooses predicted values of modal
286 abundances that minimize the sum of squared errors of prediction values for WR abundances
287 of Si, Ti, Al, Cr, Fe, Mn, Mg, Ca, Na and Ni based on EPMA data for minerals compared to
288 actual WR values for these elements. The totals of the calculated modal abundances are
289 within ±0.5% of 100% for 16 xenoliths out of 27, ±0.9% for 25 xenoliths and within ±1.2%
290 for pyroxenite 194-13 and ilmenite-bearing dunite 571-13 (ES1), possibly due to the presence
291 of unidentified accessory minerals. The modal estimates are reported in Table 1 normalized to
292 yield 100% totals. The same software has been used in our mantle xenolith studies in the last
293 two decades. Ionov et al. (2010) calculated modal compositions for three Udachnaya
294 peridotites reported by Boyd et al. (1997) using their data and the same software as in this
295 study. They reproduced four of the six modal olivine and opx values from Boyd et al. (1997)
296 within 0.1%, and obtained lower opx values (by 0.8 and 1.5%) in two samples. Overall, the
297 uncertainties of our modal estimates for olivine and opx appear to be within ±1.5%.
298
299 3.2. *Lithophile trace elements*
300 Trace elements in WR powders were determined by inductively-coupled plasma (ICP)
301 mass-spectrometry (MS) at the GIG-CAS. A multi-stage acid-digestion procedure in bombs
302 was employed for complete dissolution of acid-resistant phases like spinel and ilmenite (ES3).
303 Samples in 3% HNO_3 (1:4000 dilution) spiked with a Rh-Re solution to correct for mass-
304 related instrument drift were analyzed on a Thermo-Scientific iCAP Q with USGS reference
305 materials (BHVO-2, GSR-1, GSR-2, GSR-3, AGV-2, W-2a, SARM-4) for calibration; oxide
306 yields were <3% based on the $^{140}Ce^{16}O/^{140}Ce$ ratio. USGS basalt BIR-1 was repeatedly
307 measured as unknown and yielded abundances within ≤6% of reference values and
308 reproducibility ≤10% (2 RSD, relative standard deviation) for most elements (ES 1).
309 Trace elements in minerals were analyzed at the GIG-CAS in polished grain mounts by

310 laser ablation (LA) ICPMS with a sector field ELEMENT XR (Thermo Fisher Scientific)
311 coupled with a 193-nm (ArF) Resonetics RESOlution M-50 laser (6Hz, 4 J cm^{-2}, beam 45
312 μm). Calibration was done with USGS glasses BCR-2G, BHVO-2G and GSD-1G (external
313 standards), and Si as internal standard. Thirty analyses of TB-1G yielded abundances within
314 ≤8% of reference values and reproducibility of ≤10% (2 RSD) for most elements (ES1).
315
316 3.3. *Os isotope and HSE analyses of whole-rocks at the GIG-CAS*
317 Os isotope ratios and Re and Os abundances were determined in ~1 g of powder aliquots.
318 The samples were mixed with a ^{185}Re-^{190}Os spike, sealed into Pyrex Carius tubes with 10 ml
319 of inverse aqua regia (3:1 HNO_3:HCl) and kept at 240°C for 2 days. Osmium was extracted
320 from the aqua regia to CCl_4, then to HBr, micro-distilled using CrO_3-4N H_2SO_4, then loaded
321 onto Pt filaments and followed when dry with a $Ba(OH)_2$ activator. Os isotopic ratios were
322 measured on a Triton thermal ionization MS (TIMS) via peak hopping on single electron
323 multiplier. Data were fractionation-corrected to $^{192}Os/^{188}Os$ = 3.08271. Total Os blank was
324 0.46 ± 0.42 (2σ, n=5) pg. A mean $^{187}Os/^{188}Os$ of 0.12042 ± 0.00027 (2 σ, n=6) was obtained
325 for Merck Chemical AA standard solution for the period of analysis. These results are in good
326 agreement with a value of 0.12022 ± 0.00020 (2σ, n=14) measured on the same mass
327 spectrometer in Faraday cup mode (Li et al., 2010). Zhang et al. (2017) found no systematic
328 differences in Os isotope ratios for USGS BIR-1a digested in Carius tubes either with or
329 without de-silicification with HF prior to Carius tube digestion, indicating that an HF
330 dissolution step is not required to obtain reliable Re-Os isotope results. Our mean $^{187}Os/^{188}Os$
331 value of 0.13373±0.00081 (2σ, n=5) for BIR-1a analyzed with the same procedure is in good
332 agreement with published data (0.13372 ± 0.00080 and 0.13371± 0.00092) reported by
333 Ishikawa et al. (2014) and Zhang et al. (2017), respectively.
334 The aqua regia was dried and re-dissolved in 1N HCl after Os extraction; Re was separated

by anion chromatography (see ES3), with a cleanup column to exclude interferences. Its concentrations were measured by isotope dilution (ID) ICP-MS on a Thermo-Scientific XSERIES. Total Re blank was 6.3 ± 1.1 (2σ, n = 5) pg.

A separate aliquot of rock powder was used for PGE analyses. The concentrations of Ir, Ru, Pt and Pd were determined by ID-ICPMS after Carius tube digestion (see above) with a mixed spike containing enriched isotopes of these elements in the correct proportions for a rock with chondritic PGE ratios. Purified solutions of these elements were obtained using cation columns (see ES3) and analyzed on a Thermo Scientific iCAP-Q. Total procedural blank was <5 pg for Ir, 13 pg for Ru, 17 pg for Pd and 28 pg for Pt. Values for each element are averages of nine replicate analyses, with RSD <10% in most cases. The concentrations obtained for peridotite standards GPT-3 and GPT-4 (Chinese national reference materials GBW07290 and GBW07291) are within error of recommended values (ES3).

4. Results

4.1. *Petrography and modal composition*

Among 27 samples in this study, four are olivine megacrysts, eleven are dunites (rocks with ≥90% olivine as multiple grains), another eleven are harzburgites (52–87% olivine) and one is olivine orthopyroxenite (Streckeisen, 1976). The samples are further subdivided into four groups based on modal abundances and microstructures (Table 1; Fig. 1; ES1-2).

(1) Five megacrystalline xenoliths are distinguished by very coarse grain size of olivine (>1 cm). Four of them look like individual olivine crystals (megacrysts) that may contain inclusions of opx, cpx, garnet and spinel, e.g. U220 >8 cm long and >100 g in weight (Fig. 1b). They are comparable to seven "group 1" ($Mg\#_{Ol}$ >0.92) Udachnaya xenoliths reported by Pernet-Fisher et al. (2019), each described as "one large megacryst" of olivine, and apparently also to three samples that Pearson et al. (1995b) called "megacrystalline dunites", but are

likely olivine megacrysts as well. One of our megacrystalline samples (Uv83-13) is an aggregate of very large (>1 cm) olivine and small interstitial grains of pyroxenes, garnet and spinel, i.e. could be called megacrystalline dunite (rock composed primarily of olivine grains).

(2) Nine "coarse dunites" (Fig. 1c-f) have protogranular microstructure and consist of olivine grains 1–5 mm in size and smaller interstitial pyroxenes, garnet and spinel; sample 571-13 contains ~3% of purple ilmenite coexisting with garnet. Some contain clusters rich in garnet, spinel and opx that may have larger grain size (Fig. 1c-d). Unlike all other dunites, sample 48-12 is sheared, with irregular fragments of coarse olivine among fine-grained olivine neoblasts (Plate B', ES2). The coarse and shear dunites, unlike olivine megacrysts, have not been previously reported from Udachnaya.

(3) Nine "low-opx harzburgites" contain 11–21% opx (Fig. 1g-h) and are similar to coarse dunites in hand specimens in terms of grain size and microstructure. These harzburgites can only be distinguished from coarse dunites using modal and WR major element compositions.

(4) Two "opx-rich harzburgites" contain 40–50% opx with grain size larger than for coexisting olivine; they were added to the suite for comparison with the low-opx harzburgites. Late-stage alteration is rare or absent in nearly all the samples, which usually contain non-serpentinized olivine.

Modal compositions are given in Table 1 and shown in Fig. 2 as co-variation plots and relative to $Mg\#_{WR}$. In general, all the four main xenolith types in this study can be robustly distinguished by modal abundances. The dunites and low-opx harzburgites define a small, but distinctive gap in modal opx: ≥ 11% in the harzburgites vs. ≤5% in ten dunites out of eleven (except unusual, metasomatized sample 85-14 with 8.6% opx, Fig. 2a, d). This gap is greater than the uncertainties of modal estimates (*Section 3.1*). Olivine and opx are by far the most abundant minerals, with totals >94%, and define a linear co-variation trend for all the xenolith types, except olivine megacrysts because the latter may contain more garnet (Fig. 2c) than

opx (Fig. 2d). Garnet abundances range from 0 to 4–6% and are similar in all the rock groups (averages 2–3%, Table 1).

4.2. *Major element compositions and P-T estimates*

Major element compositions of bulk xenoliths and minerals are given in Table 2 of ES1 and shown in Figs. 3-5. The dunites, olivine megacrysts and harzburgites have similar variation ranges of some major elements (Ca, Al, Fe, Cr) as well as of Mg# in bulk samples ($Mg\#_{WR}$) (Figs. 3-4) and olivine ($Mg\#_{Ol}$). However, the bulk dunites and megacrysts tend to have higher MgO and NiO, but lower SiO_2 and Na_2O (Figs. 3e-f and 4b); they are clearly set apart from the harzburgites by higher Mg/Si_{mol} ratios (≥1.7, Fig. 3b) linked to lower modal opx in the dunites and megacrysts (Fig. 2d). The WR ranges of FeO (6.1–7.9 wt.%) and Mg# (0.917–0.934) are similar for coarse dunites, olivine megacrysts and low-opx harzburgites, and typical of those in refractory cratonic peridotites (Fig. 4a). The bulk variation ranges and average concentrations of CaO (0.13–0.47 wt.%, av. = 0.25 wt.%) and Al_2O_3 (0.02–0.68 wt.%, av. = 0.36 wt.%) for megacrystalline dunites are lower than for coarse dunites (0.28–1.04 wt. and 0.56 wt.% CaO; 0.28–1.04 wt.% and 0.56 wt.% Al_2O_3). Sheared dunite 48-12 has high FeO (12.5 wt.%) and low Mg# (0.87).

The $Mg\#_{Ol}$ for coarse peridotites and megacrysts in this study range from 0.920 to 0.934 and define a close-fitting linear co-variation with the Mg# of coexisting opx suggesting chemical equilibration, but the plots of $Mg\#_{Ol}$ vs. Mg# of garnet and cpx show more scatter (Fig. 5a). The Mg# of garnet (0.79–0.86) is much lower than for coexisting olivine and pyroxenes. The $Mg\#_{Ol}$ shows a linear correlation with $Mg\#_{WR}$ (Fig. 5c), but xenoliths with high modal abundances of low-Mg# garnet, ilmenite ($Mg\#_{Ilm}$ = 0.3) and spinel ($Mg\#_{Sp}$ = 0.53–0.75) plot off the trend to higher $Mg\#_{Ol}$; this is the reason why $Mg\#_{Ol}$ alone is not a reliable index of melt extraction for cratonic xenoliths (e.g. Doucet et al., 2013; Ionov et al.,

2010).

The modal abundances of garnet and pyroxenes are not correlated with $Mg\#_{WR}$ (Fig. 2d-f), but the garnet modes are proportional to bulk-rock Al_2O_3, in particular in dunites (Fig. 5c). The concentrations of Cr_2O_3 and the $Cr\#_{Gar}$ ($Cr/(Cr+Al)_{mol}$ in garnet) define positive correlations with the $Cr\#_{WR}$ (Fig. 5d). Together with the $Mg\#_{WR}$ vs. $Mg\#_{Gar}$ correlation, this suggests that garnet is chemically equilibrated in the peridotites, in spite of local irregularities due to zoning and distinct garnet generations. CaO in garnets shows negative correlations with MgO (close-fitting) and Cr_2O_3 (dispersed) (Fig. 5c-d).

Pressure and temperature (P-T) estimates are problematic in some xenoliths in this study because the most robust thermobarometry methods are based on compositions of coexisting pyroxenes and garnet (e.g. Nimis and Grütter, 2010), whereas not all of these minerals may be present or fully chemically equilibrated due to low abundances and/or the presence of generations with different compositions (Table 2 of ES1). Table 1 gives the list of the thermo-barometers and P-T values calculated for eleven garnet-bearing xenoliths. Temperature estimates for another ten samples that contain pyroxenes, but not garnets are based on fixed P values (3.5 or 4.0 GPa) selected using T projections to a local geotherm (Goncharov et al., 2012), and have much higher uncertainties. The P-T values for the garnet-bearing rocks (783–1154°C; 3.9–6.5 GPa) plot between the model 35 and 40 mW/m^2 conduction geotherms; the T estimates for the other xenoliths fall in the same T range (Fig. 6). Importantly, the dunites show a broad P-T range that overlaps with that earlier reported for coarse garnet peridotites from Udachnaya (Doucet et al., 2013) and thus do not appear to be concentrated within a particular depth range in the lithospheric profile.

4.3. *Trace element compositions*

Trace element compositions (and WR patterns) are given in Tables 4-5 of ES1. The WR

435 rare earth element (REE) patterns normalized to primitive mantle (PM) show continuous
436 enrichments in the light (LREE) and medium (MREE) over heavy REE (HREE), but the PM-
437 normalized abundances decrease for the heaviest REE from Lu to Tm or Ho in many samples
438 (Fig. 7a, c, d). The WR patterns for lithophile trace elements are more complex, with common
439 negative Zr-Hf anomalies and positive Nb-Ta anomalies (Fig. 7b, d, f).
440 The WR enrichments in highly incompatible elements are not likely to be due to direct
441 contamination by macroscopic veins and pockets of kimberlite, which were avoided during
442 sample preparation. Besides, the patterns for Udachnaya kimberlites and the xenoliths are
443 different for some elements like Rb, Ba, Sr (Fig. 7). On the other hand, it appears that a range
444 of kimberlite-related fluids infiltrated and reacted with the xenoliths shortly before or during
445 their transport to leave behind melt inclusions and numerous micro-phases (e.g. Golovin et
446 al., 2019). These may be alkali-carbonate liquids that reacted with host deep mantle to form
447 primitive kimberlite melts as well as mobile fractionation products of kimberlite magmas.
448 Garnet is the only accessory mineral analyzed by LA-ICPMS in many xenoliths. Its REE
449 patterns (Fig. 8) are usually sinusoidal, however garnet 565-10 has an inverted (relative to the
450 sinusoidal patterns) shape with low MREE (Fig. 8c); such patterns are common for garnets in
451 coarse Udachnaya peridotites (Agashev et al., 2013; Doucet et al., 2013; Shimizu et al.,
452 1997). The trace element data suggest that different garnet generations may be present in the
453 xenoliths. Sample 575-13 contains both the sinusoidal and LREE-depleted (Fig. 8b), but
454 HREE-MREE-enriched, garnets; the HREE-MREE-enriched patterns are typical for
455 deformed, mainly melt-metasomatized Udachnaya peridotites (Agashev et al., 2013; Doucet
456 et al., 2013).
457 Three WR dunites show positive Eu anomalies (Fig. 7a, c), but the garnets (major HREE-
458 MREE hosts) in the same samples have no sizeable Eu anomalies. Analyzing small, locally
459 zoned, garnet grains at low abundances is challenging. The Eu anomalies in the WR xenoliths

460 may be analytical artefacts due to sporadic oxide ($^{135}Ba^{16}O$) interferences with ^{151}Eu (e.g.
461 Ionov et al., 1992). Alternatively, the trace elements in the garnets may not be fully
462 equilibrated with other trace element hosts in the samples, but this is not very likely because
463 major element indices, like Mg# or Cr# (Fig. 5a, d), suggest that the garnets are equilibrated
464 with other minerals. Additional work is required to address the discrepancy.
465
466 4.4. *PGE and Re abundances*
467 The WR abundances of PGE and Re are given in Table 2. The Os concentrations in 23
468 xenoliths range from 0.4 to 15.8 ppb, about half are higher than 3.9 ppb, which is the value
469 inferred for the PM (Palme and O'Neill, 2014) whereas the sheared dunite, one low-opx and
470 two opx-rich harzburgites are very low in Os (0.01–0.04 ppb). Similar Os ranges for coarse
471 Udachnaya peridotites were previously reported by Pearson et al. (1995b) and Ionov et al.
472 (2015b). Average Os concentrations are higher for olivine megacrysts and megacrystalline
473 dunite (8.3 ± 4.5 ppb, 1σ) than for coarse dunites (4.2 ± 2.5 ppb) and low-opx harzburgites
474 (3.7 ± 1.9 ppb), but it is not clear that these differences are meaningful because the Os
475 contents are too varied (high σ), their ranges overlap and the samples are too few. The broad
476 Os variations in the xenoliths in this study are not likely to be due to the "nugget effect"
477 (sampling or analytical) alone, but may reflect heterogeneous Os distribution in the mantle on
478 a large scale, possibly due to metasomatism-related PGE mobility (e.g. Reisberg et al., 2005).
479 Re concentrations in all but four samples are at or below the PM value (0.35 ppb).
480 PM-normalized (Becker et al., 2006) patterns for PGE and Re are shown in Fig. 9. The
481 levels and patterns for Os, Ir and Ru are similar for the majority of dunites, megacrysts and
482 harzburgites, except four low-Os rocks and two other samples that have unusually high or low
483 Os/Ir ratios. Five megacrystalline xenoliths (Fig. 9a) show continuous depletions in Pt, Pd and
484 Re relative to Os, Ir, and Ru. Six coarse dunites show similar trends whereas another three

485 coarse dunites show Re-enrichments and irregular PGE patterns (Fig. 9b). The harzburgites
486 show the greatest range of patterns. All of them are depleted in Pt and Pd relative to Os-Ir-Ru,
487 but some are depleted in Pt relative to Pd and/or enriched in Re relative to Pd (Fig. 9c).
488
489 4.5. *Re-Os isotope systematics*
490 The $^{187}Re/^{188}Os$ and $^{187}Os/^{188}Os$ ratios are given in Table 2, together with $^{187}Os/^{188}Os$
491 values recalculated to the eruption age of the host kimberlite (~360 Ma) using the ^{187}Re decay
492 constant ($\lambda^{187}Re$) of $1.666 \pm 0.005 \times 10^{-11}$ a^{-1} (Smoliar et al., 1996), and model T_{RD} and T_{MA}
493 ages calculated with PM (PUM) estimates for $^{187}Os/^{188}Os = 0.1296$ (Meisel et al., 2001) and
494 $^{187}Re/^{188}Os = 0.4353$ (Becker et al., 2006); the $^{187}Os/^{188}Os$ values at the eruption age were
495 used to obtain the T_{RD} values.
496 The samples in this study define a positive $^{187}Os/^{188}Os$ vs. $^{187}Re/^{188}Os$ (Fig. 10a) linear
497 correlation ($^{187}Os/^{188}Os = 0.0062\times{}^{187}Re/^{188}Os + 0.1129$) with a slope equivalent to an age of
498 0.37 Ga, which is identical to the eruption age of host kimberlite (see *Section 2.1*). The slope
499 (hence the age) is mainly defined by a subset of ten xenoliths with very high $^{187}Re/^{188}Os$ and
500 appears to be robust, e.g. it is little affected if any of the samples with the highest $^{187}Re/^{188}Os$
501 and $^{187}Os/^{188}Os$ are removed one after another. Six of these samples are very low in Os (<0.7
502 ppb; ≤0.04 ppb in 4 samples); high $^{187}Re/^{188}Os$ (0.7–4.8) in the other four xenoliths are due to
503 a combination of high Re (0.3–0.7 ppb) and low to moderate Os. It appears that Re
504 enrichments and Os depletions are linked to processes that were coeval with, or operated
505 shortly before, the kimberlite eruption. Both T_{RD} and T_{MA} estimates for these xenoliths appear
506 to have high uncertainty and may not be well-suited to constrain their melt-extraction age; the
507 T_{MA} for these samples are very low and usually negative (Table 2).
508 Sixteen xenoliths that show no apparent Os-depletions ([Os] ≥1.8 ppb) and Re-enrichments
509 are most fitting to constrain melt extraction ages. The $^{187}Os/^{188}Os$ ratios in dunites and olivine

megacrysts among those samples (0.1066–0.1125) are lower than in harzburgites (0.1145–0.1157) while their $^{187}Re/^{188}Os$ ranges are similar (Fig. 10b). As a result, the T_{RD} ages for the dunites and megacrysts (2.4–3.1 Ga; average 2.8 Ga) are higher than for the harzburgites (1.9–2.1 Ga; average 2.0 Ga). Five megacrystalline xenoliths define a positive $^{187}Os/^{188}Os$ vs. $^{187}Re/^{188}Os$ linear correlation (Fig. 10b) with an 'isochron' age of 2.7 ± 1.2 Ga and an initial $^{187}Os/^{188}Os$ of 0.1069 ± 0.0017. The fields of dunites plus megacrysts on plots of T_{RD} ages vs. modal olivine and opx are distinct from the fields for the harzburgites (Fig. 11).

5. Discussion

5.1. *The record of melt extraction and metasomatism in the Udachnaya peridotites*

Coarse cratonic peridotites typically have high $Mg\#_{WR} \geq 0.92$ and low Al and Ca (e.g. Carlson et al., 2005), and are believed to be residues of 35–45% melting of fertile mantle at about 3 to 7 GPa based on experimental studies (e.g. Walter, 1999). Spinel harzburgites from Udachnaya were earlier interpreted as nearly pristine, in terms of modal and major oxide compositions, residues of 35–38% polybaric melt extraction (Doucet et al., 2012; Ionov et al., 2010), but garnet peridotites from Udachnaya commonly show evidence for modal metasomatism after melt extraction (Agashev et al., 2013; Doucet et al., 2013).

The content of Al_2O_3, CaO and FeO in some dunites and low-opx harzburgites in this study is about the same or even lower than in the spinel harzburgites from the earlier work (Fig. 4a) suggesting that they experienced similar, or even higher, degrees of melt extraction. Other xenoliths, however, contain more Al_2O_3 than relevant experimental melt extraction residues (Fig. 4b). The content of Al_2O_3 in our samples is not related to $Mg\#_{WR}$ (Fig. 3a), which is hard to explain in terms of Al variation due to different melting degrees, but is proportional to modal garnet (Fig. 5c). Small amounts of garnet in refractory cratonic peridotites may form by exsolution from opx on cooling after melting (Doucet et al., 2013), but dunites and olivine

megacrysts in this study contain little, if any, opx. Thus, it appears that some samples in this study experienced moderate post-melting enrichments in Al, likely linked to garnet formation, even though the content of Al_2O_3 is often considered to be a robust melt extraction index for residual peridotites (e.g. Reisberg and Lorand, 1995; Rudnick and Walker, 2009).

Clinopyroxene and ilmenite were formed by metasomatism as well; the cpx-bearing samples show enrichments in Ca (Fig. 3d) and usually have CaO $\geq Al_2O_3$ (Table 1) while the ilmenite-bearing xenoliths have $TiO_2 \geq 0.06$ wt. %.

Very low HREE contents in the dunites, megacrysts and low-opx harzburgites (0.01–0.1 × PM; Fig. 7) and PM-normalized values that decrease from Lu up to Ho (i.e. in the direction of lower compatibility) also suggest that the protoliths for these xenoliths formed by high-degree melt extraction. However, trace element data, e.g. WR patterns with remarkably regular enrichments from HREE to MREE and LREE, suggest that all the xenoliths were subsequently affected by post-melting metasomatism, in line with the common presence of metasomatic garnet, cpx and ilmenite. The LREE are positively correlated with CaO and may be mainly hosted in Ca-rich accessory phases. Megacrystalline xenoliths show the largest REE range, but coarse dunites have higher average LREE-MREE as a group (Fig. 7). MREE-LREE enrichments were reported for olivine separated from Udachnaya megacrysts (Pernet-Fisher et al., 2019) as well, but at concentrations an order of magnitude lower.

A dunite and a harzburgite, in which ilmenite was found in thin sections and/or crushed rocks, have the highest positive Nb-Ta anomalies (Fig. 7), suggesting that the Nb-Ta enrichments in several other xenoliths in this study may be due to accessory metasomatic ilmenite as well. Occasional Sr enrichments may suggest the presence of mantle-derived carbonates (e.g. Ionov, 1998), like those in xenoliths from Obnazhennaya (Ionov et al., 2018b), but no carbonates were found in thin sections.

559 The origin of dunites and megacrystalline olivine in cratonic mantle remains controversial.
560 Dunite formation has been attributed to high-degree melting either in nominally anhydrous
561 upwelling mantle (ancient plumes or spreading environments) (e.g. Herzberg, 2004; Servali
562 and Korenaga, 2018), or in subduction zones and their Archean equivalents supposing that the
563 presence of water may enhance melting (Liu et al., 2018; Pearson and Wittig, 2008; Wittig et
564 al., 2008). Bernstein et al. (2006) reported dunite and low-opx harzburgite xenoliths from
565 West Greenland (too small to obtain WR samples) with the ranges of $Mg\#_{Ol}$ (0.920–0.937)
566 and $Cr\#_{Spl}$ (0.47–0.96) similar to those in this study, and suggested that these rocks formed by
567 dry melting to the point of opx exhaustion in the Archean. By contrast, Pearson and Wittig
568 (2008) argued for the presence of water during melting to form dunites from another West
569 Greenland site and speculated that migration of siliceous melts produced by opx breakdown
570 may produce opx-rich harzburgites, like those in this study and earlier work on Udachnaya
571 (Boyd et al., 1997; Doucet et al., 2012; Ionov et al., 2010). Alternatively, dunite formation in
572 mantle lithosphere was attributed to reaction of harzburgites with migrating mafic melts that
573 breaks down and removes opx (e.g. Kelemen et al., 1990). The origin of megacrystalline
574 olivine remains a mystery.
575 The Re-Os dating of xenoliths in this study provides an important argument in this debate
576 by establishing that Udachnaya dunites and olivine megacrysts are systematically older than
577 low-opx harzburgites. For instance, the Udachnaya dunites cannot be melt channel materials
578 (Kelemen et al., 1990), by contrast to dunites hosted by the Obnazhennaya kimberlite in the
579 NE Siberian craton that have younger T_{RD} ages and lower Mg# than harzburgites (Ionov et
580 al., 2015a). Similarly, the Udachnaya dunites and olivine megacrysts cannot have been
581 produced by re-melting in subduction zones of older harzburgites formed in ocean ridge
582 settings (Pearson and Wittig, 2008). Finally, the change in modal compositions from Archean
583 dunites to Proterozoic harzburgites cannot be attributed to cooling of the mantle after the late

584 Archean (Herzberg et al., 2010) because they have similar Mg#, Al and Ca ranges, but
585 distinct Mg/Si ratios (Fig. 3), and because harzburgites in other cratons usually have Archean
586 ages.
587
588 5.2. *The distribution of PGE and Re in the mantle beneath Udachnaya*
589 This study provides the first HSE data for coarse WR dunites and an orthopyroxenite from
590 Udachnaya as well as for bulk large olivine megacrysts rather than their fragments or pure
591 olivine. The abundances and patterns of HSE in 17 WR coarse harzburgites (as well as in
592 lherzolites and deformed peridotites) from Udachnaya were reported by Ionov et al. (2015b);
593 they are generally similar to those in this study. Literature data for olivine separated from
594 small Udachnaya peridotite xenoliths often show very low Os concentrations (Pearson et al.,
595 1995b; Pernet-Fisher et al., 2015) apparently because pure olivine is very low in Os (e.g.
596 Burton et al., 2000) and because Os hosts (alloy and sulfide micro-phases) may be unevenly
597 distributed (e.g. Aulbach et al., 2016). By comparison, reported Os concentrations in
598 fragments of eight high-Mg# olivine megacrysts from Udachnaya (Pearson et al., 1995b;
599 Pernet-Fisher et al., 2019) are consistently high (0.4–10.7 ppb; av. = 4.4 ± 4.0 ppb (1σ)) and
600 overlap those for coarse dunites and bulk megacrysts from this study (Plate 6, ES1). We posit
601 that Os in coarse peridotites including dunites reside mainly in intergranular micro-phases,
602 while Os in megacrystalline olivine-rich xenoliths may be hosted by inclusions in olivine.
603 Experimental evidence and studies of natural samples have shown that Os and Ir are
604 compatible during partial melting of fertile mantle and that as melting proceeds move from
605 sulfides into Os-Ir alloys in refractory residues (e.g., Brenan and Andrews, 2001). By
606 contrast, Pt and Pd are compatible to slightly incompatible at low to moderate melting
607 degrees, but are largely extracted from the residues after 20–25% of melting when sulfides are
608 exhausted (e.g. Pearson et al., 2004). The HSE concentrations and patterns in megacrystalline

609 xenoliths and the majority of coarse dunites and low-opx harzburgites in this study (Fig. 9)
610 are consistent with well-known HSE behavior during melt extraction. The Os, Ir and Ru
611 concentrations in these samples are close to or somewhat higher than in PM as expected from
612 mass-balance calculations for compatible elements in melting residues and commonly
613 observed in cratonic peridotites (Aulbach et al., 2016; Ionov et al., 2015b; Pearson et al.,
614 2004). By contrast, PM-normalized Pt, Pd and Re abundances in the majority of the samples
615 decrease steadily due to incompatible behavior at high melting degrees.
616 Seven coarse dunites and harzburgites (including two high-opx harzburgites) show
617 complex HSE patterns in Fig. 9. All of them have high Re/Os ratios, six are enriched in Re
618 over Pt-Pd and four are very low in Os. As shown in *Section 4.5* and Fig. 10a, these samples
619 define a positive linear $^{187}Re/^{188}Os$ vs. $^{187}Os/^{188}Os$ correlation corresponding to the eruption
620 age of host kimberlite, and close to those obtained by Pearson et al. (1995b) and Ionov et al.
621 (2015b) for Udachnaya peridotites with high Re/Os ratios. We see this as evidence that both
622 the Re enrichments and PGE mobility are caused by some kind of interaction of the rocks
623 with kimberlite-related media, most likely shortly before the transport of the xenoliths by
624 kimberlite eruption, as shown earlier for sheared Udachnaya peridotites (Golovin et al., 2018;
625 Golovin et al., 2019). By contrast, we see no robust evidence in hand specimens, thin sections
626 or chemical analyses for intrusion of the WR samples by bulk kimberlite material during the
627 eruption. For instance, Re concentrations in the kimberlites (0.11–0.16 ppb) (Ionov et al.,
628 2015b) are too low to account for Re enrichments in the xenoliths; some trace element ratios
629 in the kimberlites are different from those in the xenoliths (Fig. 7; see *Section 4.3*).
630 The fact that no low-Os, high-Re samples are found among megacrystalline xenoliths
631 may be related to their unusually large grain size, hence low permeability. Two opx-rich
632 harzburgites analyzed are very low in Os, but they are too few to infer that this is typical for
633 this rock type. Ionov et al. (2015b) found seven low-Os xenoliths among 29 Udachnaya

peridotites analyzed; all of them were garnet- and cpx-bearing harzburgites affected by modal metasomatism. They speculated that at some conditions (high T, specific melt compositions, oxygen fugacity) metasomatism may mobilize and remove Os and other PGE from refractory residues (e.g. Aulbach et al., 2016; Wittig et al., 2010a). Because all the low-Os coarse Udachnaya peridotites are Mg-rich (Mg# 0.922–0.934), the hypothetical percolating melts must have high Mg# and/or be low in iron (e.g. Na-Ca-Mg carbonatites). On the other hand, PGE+Re patterns in many strongly metasomatized xenoliths in this study (e.g. ilmenite-bearing and those with the highest modal garnet, cpx and LREE) are not perturbed.

The origin of sheared dunite 48-12 that has both low PGE abundances and low Mg# is uncertain. Its lithophile trace element pattern is very similar to that of olivine megacryst U220 (Plate 4a, ES1). Sheared Udachnaya peridotites reported by Ionov et al. (2015b) have higher PGE concentrations, and some have nearly flat, PM-like PGE+Re patterns. These rocks have high Pt-Pd and Re abundances in spite of (or due to?) melt-metasomatism (e.g. Luguet et al., 2015) that accompanied shearing in these rocks. Olivine orthopyroxenite 194-13, which most likely is of magmatic origin, has a convex-up PGE+Re pattern with maxima for Ru and Pt.

5.3. *Constraints on the use of Re-Os isotope data for melt-depletion age estimates*

Constraining the age of the xenoliths involves several types of uncertainties. One of them relates to ubiquitous post-melting Re-enrichments, which are commonly linked to processes coeval with the eruption of host magma. This is a problem common to Re-Os studies of xenoliths that led to the definition of the Re-depletion model age (T_{RD}: Walker et al. (1989)). T_{RD} ages are calculated by first correcting the $^{187}Os/^{188}Os$ ratios measured in each sample back to the age of the host volcanic rock using each sample's Re/Os ratio to account for any Re-addition that presumably occurred at the time of the eruption. The calculated initial $^{187}Os/^{188}Os$ is then compared with the Os isotope evolution of pristine undifferentiated mantle

assuming that the sample had a Re/Os ratio of zero prior to its capture by the host magma. If the sample had a non-zero Re/Os ratio while still in the mantle, the T_{RD} approach provides only a minimum estimate to the time of Re-depletion through melt extraction.

This approach works well for xenoliths with relatively low Re/Os ratios, but its ambiguity increases with increasing Re/Os ratios measured in a sample, and also depends on (a) the exact knowledge of the eruption age and (b) the absence of pre-eruption Re enrichments. Nearly all the samples in this study are highly refractory melt extraction residues (*Section 5.1*), and it is reasonable to assume that they had negligible Re abundances after their formation and thus are likely to yield robust melt extraction age estimates. Very high $^{187}Re/^{188}Os$ (up to 4.8) of several xenoliths in this study result in large, and hence uncertain, eruption age corrections for $^{187}Os/^{188}Os$ and T_{RD} values. We evaluated uncertainties related to the eruption age of the host kimberlite (~360 Ma) by recalculating initial $^{187}Os/^{188}Os$ ratios with eruption ages of 390 Ma and 330 Ma for the xenoliths with high Re/Os ratios and obtained significant T_{RD} variations ranging from ±0.06 Ga for sample 615-09 to ±0.3 Ga for sample 63-13. Re enrichments by ancient metasomatism may affect T_{RD} estimates even more.

To minimize such uncertainties, we disregard T_{RD} estimates for samples with $^{187}Re/^{188}Os$ ratios higher than the PM value (0.435; Becker et al. (2006)) as well as for dunite 85-14 because its $^{187}Os/^{188}Os$ ratio is too radiogenic for an ancient melt extraction residue and more consistent with Re enrichments long before the kimberlite eruption. Altogether, we examine below the age estimates for five low-opx harzburgites and eleven dunites and megacrysts, $^{187}Re/^{188}Os$ in these samples ranges from 0.02 to 0.13 (Table 2).

Uncertainties in Re-Os model ages are also related to the choice of different models for the hypothetical undifferentiated upper mantle reservoir (Bulk Silicate Earth, BSE) that was melted to yield residual mantle peridotites. The T_{RD} and T_{MA} ages in this study are calculated with the commonly used primitive upper mantle (PUM or PM) model based on fertile mantle

684 peridotites: $^{187}Os/^{188}Os$ = 0.1296 ± 0.0008 (Meisel et al., 2001) and $^{187}Re/^{188}Os$ = 0.435 ±
685 0.010 (Becker et al., 2006). An earlier version of this model reported a slightly lower
686 $^{187}Os/^{188}Os$ of 0.1290 (Meisel et al., 1996).
687 Alternative BSE models are based on the compositions of different groups of chondrites.
688 Shirey and Walker (1998) reported present-day chondritic reference values of $^{187}Os/^{188}Os_{ch}$ =
689 0.127 and $^{187}Re/^{188}Os_{ch}$ = 0.40186. Walker et al. (2002a) showed that carbonaceous
690 chondrites have a distinctively low average $^{187}Os/^{188}Os$ (0.1262 ± 0.0006; $^{187}Re/^{188}Os$ = 0.392
691 ± 0.015) while enstatite ($^{187}Re/^{188}Os$ = 0.421 ± 0.013; $^{187}Os/^{188}Os$ = 0.1281 ± 0.0004) and
692 ordinary ($^{187}Re/^{188}Os$ = 0.422 ± 0.025; $^{187}Os/^{188}Os$ = 0.1283 ± 0.0017) chondrites overlap with
693 a mean of 0.1282. The latter value is within error of the Os isotopic composition of
694 convecting upper mantle deduced from ophiolite chromites ($^{187}Os/^{188}Os$ = 0.1281 ± 0.0009;
695 (Walker et al., 2002b)). If the PUM composition was set via addition of a late veneer of
696 planetesimals, it appears that the veneer was dominated by ordinary and enstatite chondrites.
697 Incorrect use of the model parameters may lead to erroneous T_{RD} and T_{MA} values and
698 considerable confusion in comparison of mantle formation ages, e.g. as shown recently for
699 xenoliths from Obnazhennaya in the NE Siberian craton (Ionov et al., 2018a). The differences
700 in T_{RD} ages based on contrasting BSE models for ≥3 Ga old cratonic peridotites may be as
701 high as 0.3 Ga (e.g. Carlson et al., 1999). BSE reference values in some previous Re-Os work
702 on Udachnaya xenoliths are different from those in this study. Pearson et al. (1995b) used
703 ^{187}Re decay constant = 1.64×10^{-11} a^{-1}, $^{187}Re/^{188}Os$ = 0.397 and $^{187}Os/^{188}Os$ = 0.12757. Pernet-
704 Fisher et al. (2015) and Pernet-Fisher et al. (2019) used the chondrite average from Shirey and
705 Walker (1998) for $^{187}Os/^{188}Os$ = 0.127, but a $^{187}Re/^{188}Os$ = 0.3935 (CV3 chondrite Allende ?).
706 The model ages from these papers were recalculated using the PUM model (Plate 6 of ES1)
707 for comparison with data in this study. In addition, Table 2 shows T_{RD} and T_{MA} for samples in
708 this study calculated with the chondritic model of Shirey and Walker (1998); the differences

709 in model ages using the two BSE models are ≤0.2 Ga for nearly all the samples (ES1).

710

711 5.4. *Formation age of refractory lithospheric mantle in the central Siberian craton*

712 T_{RD} ages for low-opx harzburgites (1.9–2.1 Ga; average 2.0 ± 0.1 Ga (1 σ)) are manifestly
713 younger than for dunites and olivine megacrysts (2.4–3.1 Ga; av. 2.8 ± 0.2 Ga) among the 16
714 low-Re/Os xenoliths in this study deemed most fitting for T_{RD} age estimates. All these
715 samples also yield coherent T_{MA} values, which are slightly older than the T_{RD} ages, with T_{MA}
716 averages of 2.2 ± 0.3 Ga for the harzburgites and 3.2 ± 0.2 Ga for the dunites and olivine
717 megacrysts. By contrast, T_{MA} for the high-Re/Os samples are very low and usually negative
718 (Table 2). As discussed in the previous section, we consider that T_{RD} estimates for such
719 samples cannot be viewed as robust melt extraction ages because the effects of Re addition by
720 post-melting processes are too large to be accurately corrected. The T_{RD} range for all nine
721 low-opx harzburgites in this study (including four high-Re/Os samples) is much wider (1.5–
722 2.4 Ga), but the average (2.0 ± 0.3 Ga) is not very different from that obtained for samples
723 with low Re/Os alone. Overall, the screening procedure to discard samples with perturbed
724 Re/Os ratios allows to better constrain the T_{RD} range for the harzburgites by reducing the data
725 scatter, and thus to clearly discern it from the T_{RD} range for the dunites and megacrysts (Figs.
726 10-12).

727 Previous work on Re-Os dating of Udachnaya peridotite xenoliths reported a much greater
728 proportion of samples with high Re/Os ratios than in this study, hence potentially more T_{RD}
729 scatter. $^{187}Re/^{188}Os$ in eight coarse peridotites reported by Pearson et al. (1995b) range from
730 0.23 to 27; four of these samples have $^{187}Re/^{188}Os$ ≤1.5 and yield Paleoproterozoic T_{RD} (2.0–
731 2.2 Ga; av. 2.1 ± 0.1) calculated with the PUM model as in this study (Table 6 of ES1). Ionov
732 et al. (2015b) reported nine coarse harzburgites with $^{187}Re/^{188}Os$ from 0.13 to 2.5 and T_{RD}
733 from 1.4 to 2.2 Ga, and chose six of them as best representing melt extraction ages (2.0–2.2

734 Ga; av. 2.1 ± 0.1 Ga). The data from previous studies overlap the T_{RD} range for low-opx
735 harzburgites in this study (1.9–2.1 Ga; av. 2.0 ± 0.1 Ga) obtained on samples with $^{187}Re/^{188}Os$
736 ≤0.126, which we consider the best current age estimate for this rock type (Fig. 12a). Overall,
737 the Paleoproterozoic formation at ~2 Ga for coarse harzburgites, which make up the greatest
738 portion of the refractory protolith of lithospheric mantle beneath Udachnaya, is now firmly
739 established by several studies and cannot be ignored when discussing the age and history of
740 the Siberian craton.
741 This study is the first to identify and characterize coarse (≤5–10mm) dunites, as defined in
742 *Section 4.1*, i.e. distinct from previously reported olivine megacrysts and "megacrystalline
743 dunites", among Udachnaya xenoliths. The coarse dunites are hard to tell from low-opx
744 harzburgites in hand specimens and were identified here using modal and major oxide
745 abundances. Coarse dunites are nearly impossible to recognize in the field, and can be easily
746 overlooked. By contrast, megacrystalline xenoliths can be set apart in hand specimens and in
747 the field based on olivine ≥1 cm. The T_{RD} ranges and averages for olivine megacrysts (2.4–
748 3.0 Ga, av. 2.6 ± 0.2 Ga) and coarse dunites (2.5–3.1 Ga, av. 2.9 ± 0.2 Ga) in this study are
749 not very different (within ~1σ for averages) (Fig. 12a). If these two xenolith types have
750 different origins and formed in distinct events, their formation may be roughly coeval.
751 The meaning of the 'isochron' defined by the megacrystalline xenoliths in Fig. 10b is not
752 clear. One option could be to ascribe the isochron to an event ~2.7 Ga ago that produced a
753 range of Re/Os ratios in parts of a protolith with an initial $^{187}Os/^{188}Os$ of 0.1069 that have
754 since developed the $^{187}Os/^{188}Os$ values measured in these samples. In such a case, the
755 formation age of the megacrystalline suite in this study could be ~2.7 Ga, not much different
756 from its average T_{RD} of 2.6 ± 0.2 Ga (Table 2). However, this isochron age is too uncertain
757 because of high error (±1.2 Ga) to warrant such an inference.
758 Alternatively, based on model ages in the combined dunite and megacryst population (Fig.

759 12a), they can be grouped in two subsets with much more tightly clustered ages: six samples
760 with the T_{RD} range of 2.4–2.7 Ga (av. 2.6 ± 0.1 Ga) and five with the T_{RD} range of 2.8–3.1 Ga
761 (av. 3.0 ± 0.1 Ga). Average T_{MA} estimates for the same xenoliths are 3.0 ± 0.2 Ga and 3.3 ±
762 0.1 Ga. The average T_{RD} ages in these two clusters are distinct within ±2σ, which may imply
763 that they formed in two distinct Archean events. In such a case, the difference in grain size
764 between the megacrysts and coarse dunites may not be related to age, and possibly unrelated
765 to the formation mode of their protoliths.
766 Pearson et al. (1995b) reported Re-Os data on five "megacrystalline peridotites" that have
767 0.6–2.6 ppb Os, $^{187}Re/^{188}Os$ of 0.12–0.97 and T_{RD} of 1.9–2.8 Ga (re-calculated with the PUM
768 model, Table 6 of ES1). The T_{RD} in these samples fall in two groups: ~1.9 Ga and 2.8–3.2 Ga;
769 the latter range is only slightly higher than for dunites and megacrysts in this study (Fig. 12a).
770 These results are hard to compare directly with our dataset because they were obtained not on
771 representative WR samples, like in this study, but on small amounts of material extracted
772 from xenoliths, for which no other data were reported, except that their $Mg\#_{Ol}$ range
773 overlapped that for coarse peridotites from the same suite.
774 Pernet-Fisher et al. (2019) obtained Archean T_{RD} values (2.5–3.1 Ga, av. = 2.9 ± 0.2 Ga;
775 re-calculated with the PUM model, Plate 6 of ES1) for pure olivine separated from seven
776 megacrysts with Mg# >0.92 from Udachnaya, and aberrant T_{RD} for megacrysts with lower
777 Mg#. The T_{RD} ranges and averages for the Mg-rich olivine are similar to those for megacrysts
778 (as well as dunites) in this study (Fig. 12a). By contrast, olivine separated from many
779 peridotite xenoliths from Udachnaya and Obnazhennaya (Pernet-Fisher et al., 2015) showed
780 low Os, high Re/Os and invalid Re-Os model ages contrary to the commonly held view that
781 olivine provides a good measure of whole rock Re-Os systematics in peridotites (see also
782 Ionov et al., 2015a). The olivine separates from Udachnaya megacrystalline xenoliths have
783 consistently high Os concentrations as well (*Section 5.2*), which may suggest that Os in these

megacrysts is hosted by micro-inclusions in olivine, which may make them adequate for T_{RD} estimates, unlike for peridotite xenoliths where much Os may be hosted by intergranular materials.

5.5. *Multi-stage formation of the Siberian craton*

This study firmly establishes that various dunites are the oldest peridotites in the mantle beneath Udachnaya, in addition to earlier work that reported Archean (as well as younger) T_{RD} ages for olivine megacrysts and samples designated as "megacrystalline dunites" with unknown modal and bulk chemical compositions (Pearson et al., 1995b; Pernet-Fisher et al., 2019). To evaluate the role of dunites and megacrystalline olivine in the origin and evolution of the lithospheric mantle it is important to constrain their abundance and position in the lithosphere. The dunites and megacrysts in this study come from a broad depth range (≤120–210 km; Fig. 6) and are not restricted to a particular lithospheric layer. Russian sources cited by Boyd et al. (1997) estimated the proportion of "megacrystalline peridotites" at ~3% of Udachnaya xenolith population without specifying how the value was obtained. This estimate appears to be exaggerated. Shiny, coarse olivine crystals draw more attention than other xenolith materials and may seem more common. Our field data suggest that dunites and olivine crystals >2–3 cm in size are very rare in Udachnaya-East kimberlites and much smaller than xenoliths of other peridotites and eclogites, consistent with the absence of bulk analyses of "megacrystalline dunites" in the literature. Their mass proportion among mantle xenoliths may be very low.

Boyd et al. (1997) speculated that very coarse peridotites are rare among Udachnaya xenoliths because they disintegrate during eruption faster than fine-grained rocks. We see no reason to suppose that "megacrystalline dunites" are less solid than rocks with smaller grain size or less olivine; the opposite may be true. Fine-grained, sheared peridotites may be

809 abundant among Udachnaya xenoliths not because they are more solid, but because they form
810 in the vicinity of magma feeders due to interaction with proto-kimberlite melts, hence are
811 more likely to be captured by the magma when eruption starts (e.g. Doucet et al., 2014).
812 Because harzburgites are by far the most common type of coarse peridotites among
813 Udachnaya xenoliths, the main part of the existing mantle lithosphere beneath Udachnaya
814 formed in the Paleoproterozoic, as previously suggested by Ionov et al. (2015b). This study
815 offers more precise age estimates for this event constrained by the T_{RD} range for low-opx
816 harzburgites (Table 2): 1.9–2.1 Ga (average 2.0 ± 0.1 Ga) based on the PUM model, and 1.8–
817 2.0 Ga (average 1.9 ± 0.1 Ga) based on the chondrite model of Shirey and Walker (1998).
818 Further support for the Paleoproterozoic formation age comes from Lu-Hf model and
819 isochron ages (1.7–1.9 Ga) reported by Doucet et al. (2015) for cpx-bearing spinel
820 harzburgites as well as Re-Os dating of sulfide inclusions in diamonds from Udachnaya,
821 which yield 1.8 Ga isochron ages (Wiggers de Vries et al., 2013).
822 This study further indicates that, given the predominance of Paleoproterozoic ages for the
823 most typical lithospheric peridotites from Udachnaya, the rare older components may be relict
824 materials, i.e. fragments of ancient lithospheric mantle formed in the Archean that were
825 incorporated into cratonic roots during the final assembly of the central Siberian craton in the
826 Paleoproterozoic (Ionov et al., 2015b; Moyen et al., 2017). Our data give new insights into
827 the earliest lithospheric formation stages in the central Siberian craton.
828 Our preferred interpretation of the Re-Os model ages for the dunites and megacrysts in
829 this study is that they record two distinct Archean events, one in the Neoarchean and the other
830 one in the early Mesoarchean. The lower age limits for these two events are constrained by
831 the T_{RD} values (2.6 ± 0.1 Ga and 3.0 ± 0.1 Ga) and the upper age limits by the T_{MA} values (3.0
832 ± 0.2 Ga and 3.3 ± 0.1 Ga). The mean T_{RD} ages of ~2.6 and ~3.0 Ga (Fig. 12a) may be closer
833 to true values considering that Re in these highly refractory samples must be dominated by

post-melting additions. Model ages calculated using the BSE model of Walker et al. (2002a), based on ordinary and enstatite chondrites, are only slightly lower with the T_{RD} of 2.5 ± 0.1 Ga and 2.9 ± 0.1 Ga and the T_{MA} of 2.9 ± 0.1 Ga and 3.2 ± 0.1 Ga. These two age groups comprise both coarse dunites and megacrystalline xenoliths suggesting no links between olivine grain size and age, contrary to speculations in earlier work (Pearson et al., 1995b).

Sobolev et al. (1984) and Pokhilenko et al. (1993) asserted that many megacrystalline dinites contain diamonds (none has been found in samples from this study). Because diamond formation in peridotites is commonly linked to metasomatism, the large olivine grain size in this rock type could be linked to reworking and recrystallization of coarse dunites. Re-Os ages of sulfide inclusions in Udachnaya diamonds (Wiggers de Vries et al., 2013) indicate that this may have happened ~0.2 Ga after the major stage of lithospheric formation at 2.0 Ga, which appears to be a reasonable time for thickening and cooling of initial melting residues to allow for diamond formation at depths ≥130 km (Fig. 6).

A prolonged, multi-stage formation of the Siberian lithospheric mantle is consistent with recent data on crustal basement ages. U-Pb zircon ages for crustal xenoliths from Udachnaya (Moyen et al., 2017) show that lower crustal granulites formed in the Proterozoic (1.83–1.87 Ga) whereas tonalities and other upper crustal rocks formed in the Archean (2.71–2.73 Ga). They inferred that the deep lithosphere beneath Udachnaya did not form in a single Archaean event, but grew in at least two distinct events, first in the late Archaean, then in the Paleoproterozoic when a large-scale delamination and rejuvenation of the Archaean lower crust and lithospheric mantle took place. The crustal xenoliths show no evidence for Mesoproterozoic crustal formation (Fig. 12b), and thus do not support mantle melting at ~1.2 Ga evoked by Pernet-Fisher et al. (2015).

The crustal basement in the central Siberian craton is hidden under a thick sedimentary cover, but is exposed on the Anabar shield in the north (KML file), which appears to belong

859 to the same tectonic unit (Daldyn block) as Udachnaya (Rosen, 2002). Zircons in modern
860 sediments from the Anabar shield (Paquette et al., 2017) define three U-Pb age ranges: 3.0–
861 3.4 Ga, 2.4–2.8 Ga and 1.8–2.0 Ga, with the youngest event linked to the amalgamation of the
862 craton by welding of Archean domains. Similar U-Pb ages were obtained for detrital zircons
863 from Meso- and Neoproterozoic sedimentary basins at the western (2.6–2.5 and 1.9–1.85 Ga)
864 and NE (2.9–2.7 and 2.1–1.95 Ga) margins of the craton (Priyatkina et al., 2016).

865 To sum up, the U-Pb zircon ages from the crustal basement outline three main stages of
866 crustal growth in the northern and NE Siberian craton: 3.0–3.4 Ga, 2.4–2.8 Ga and 1.8–2.0
867 Ga, with the number of zircons increasing from the older to younger ages (Fig. 12b). These
868 stages overlap the three intervals of lithospheric mantle formation (melt extraction) for
869 refractory peridotites in this study (Fig. 12a,b). This conclusion is robust relative to the
870 uncertainties related to Re-Os dating of mantle peridotites, i.e. T_{RD} versus T_{MA} ages and the
871 PUM vs. chondritic BSE composition models. Overall, similarities of U-Pb ages of zircons
872 from the crustal basement and formation ages of refractory peridotites in this study suggest
873 temporal coupling, and possibly genetic links, between crust and mantle formation in the
874 building of the cratonic lithosphere beneath the central Siberian craton (Moyen et al., 2017).

875 An intriguing question, to which we may not have an answer as yet, is if the Udachnaya
876 dunites have preserved the modal and chemical composition of the original Archean mantle
877 lithosphere, or alternatively, were extensively modified during its disruption and reworking in
878 the Paleoproterozoic. The distribution and composition of peridotite xenoliths with Archean
879 ages at Udachnaya are different from those in the Obnazhennaya kimberlite at the NE margin
880 of Siberian craton where Paleoproterozoic and Archean peridotites occur in similar
881 proportions and have similar compositions (Ionov et al., 2015a). On the other hand, the
882 lithospheric mantle compositions and ages may differ in different parts of the Siberian craton.

883 Another unresolved question is how the minor domains of Archaean lithospheric mantle

were intercalated with the dominant Proterozoic lithospheric mantle during Siberian craton assembly. Most likely, the Archaean domains (including eclogites (Pearson et al., 1995c)) were thrusted into the Proterozoic mantle via complex tectonic displacement of portions of the lithospheric mantle during Paleoproterozoic orogeny or underplating (Liu et al., 2016; Wang et al., 2018). Alternatively, the olivine-rich materials in this study could be recycled fragments of Archean cratonic roots, first delaminated then incorporated in the Proterozoic lithospheric mantle by upwelling asthenosphere.

5.6. *Not all cratonic mantle is Archean*

Early Re-Os studies of coarse peridotites from cratons in South Africa and North America provided mainly Archean T_{RD} ages (Carlson, 2005; Pearson, 1999) and were seen as evidence that cratonic lithospheric mantle only formed in the Archean. As a result, the terms 'Archean' and 'craton' are often considered essentially synonymous, i.e. the lithospheric mantle in all cratons is presumed to have formed in the Archean. However, data compilations (Doucet et al., 2015; Wittig et al., 2010b) show that a significant proportion of peridotites from the Slave and North Atlantic cratons record T_{RD} ages of 1.8–1.9 Ga matching major crust generation events in those cratons. The central Siberian craton is the first proven case of a craton whose lithospheric mantle formed essentially in the Paleoproterozoic (Ionov et al., 2015b), concomitant with major crust formation or rejuvenation events (Moyen et al., 2017; Paquette et al., 2017). Lithospheric peridotites at the NE margin of the Siberian craton have both Archean and Paleoproterozoic ages (Ionov et al., 2015a) (Fig. 12a).

Recent Re-Os studies of peridotite xenoliths in kimberlites from Arctic Canada have provided other examples of cratons with Paleoproterozoic mantle roots. Liu et al. (2018) reported ~2 Ga T_{RD} ages for peridotites from diamond-bearing kimberlites at the Parry Peninsula and Central Victoria Island, whose mineral and whole rock chemistry is

909 indistinguishable from that of typical cratonic mantle lithosphere. Kimberlite-borne peridotite
910 xenoliths from the central Rae craton (Liu et al., 2016) show both Archean and 2.1–1.7 Ga
911 ages; the Paleoproterozoic peridotites are interpreted to represent juvenile lithospheric mantle
912 that replaced and/or mixed with the lower portion of Archean lithospheric mantle to form
913 thick lithospheric roots extending well into the diamond stability field. Overall, the new data
914 place the final limit for the formation of cratonic lithosphere with specific modal and
915 chemical compositions, and the transition from the 'Archean' to modern tectonic regimes, at
916 2.0 Ga, rather than at the Archean-Proterozoic boundary as is commonly thought. By contrast,
917 we see no robust evidence from appropriate refractory peridotite xenoliths (representative WR
918 samples, undeformed, high-Mg, low Re/Os) to support speculations (Pernet-Fisher et al.,
919 2015) on even younger (Mesoproterozoic) melt extraction ages in the lithospheric mantle of
920 the central Siberian craton (Fig. 12).
921
922 **6. Conclusions**
923 (1) The Udachnaya kimberlite in the central Siberian craton hosts very rare, small fragments
924 of previously unreported coarse and sheared dunites as well as megacrystalline xenoliths
925 (olivine >1–2 cm), equilibrated at 783–1154°C and 3.9–6.5 GPa (~120–220 km).
926 (2) The coarse dunites, olivine megacrysts and low-opx harzburgites have similar bulk
927 variation ranges of Ca, Al, Fe, Cr and Mg# (0.917–0.934) typical of refractory cratonic
928 peridotites, but the dunites and bulk megacrysts have higher MgO, NiO and Mg/Si_{mol}
929 ratios. Modal abundances and those of Ca and Al are not correlated with $Mg\#_{WR}$, and may
930 not be due to differences in melting degrees.
931 (3) Some xenoliths show high $^{187}Re/^{188}Os$ positively correlated with $^{187}Os/^{188}Os$ consistent
932 with the eruption age of host kimberlite (0.37 Ga). The Os depletions and enrichments in
933 Re and other incompatible elements may be linked to fluids related to the generation and

fractionation of kimberlite liquids that were coeval with, or operated shortly before, the kimberlite eruption.

(4) Robust T_{RD} ages for 16 low-$^{87}Re/^{188}Os$ (0.02–0.13) xenoliths are distinctly lower for harzburgites (1.9–2.1 Ga; average 2.0 ± 0.1 Ga) than for dunites and olivine megacrysts (2.4–3.1 Ga; av. 2.8 ± 0.25 Ga). The dunites and megacrysts define two subsets with average T_{RD} of 2.6 ± 0.1 Ga and 3.0 ± 0.1 Ga, and T_{MA} of 3.0 ± 0.2 Ga and 3.3 ± 0.1 Ga. The difference in grain size (medium- to coarse-grained dunites vs. megacrystalline xenoliths) is not related to age. Thus, the dunites or olivine megacrysts could not be produced by re-melting of harzburgites, nor be melt channel materials in harzburgites.

(5) The dunites are relict fragments of lithospheric mantle formed in two Archean events (at or soon after 2.6 and 3.0 Ga) and incorporated into present mantle lithosphere during the final assembly of the Siberian craton in the Paleoproterozoic. These formation ages of the mantle lithosphere are consistent with crustal basement ages from U-Pb dating of zircons.

(6) The new data from Siberia and other cratons suggest that the formation of cratonic lithosphere with specific modal and chemical compositions did not stop at the Archean-Proterozoic boundary as is commonly thought, but continued in the Paleoproterozoic.

Acknowledgements

We thank the ALROSA joint stock company and the open pit mine staff for access to the site and assistance with sample collection. DAI and ZL thank P. Nimis for assistance with P-T estimates. This study was financially supported by the Strategic Priority Research Program of the Chinese Academy of Sciences (XDB18000000) and the National Natural Science Foundation of China (41688103). AVG was supported by the Russian Science Foundation (project No. 18-77-10062); AVK was supported by the Russian Federation state assignment project of IGM SB RAS. DAI acknowledges Chinese Academy of Sciences President's

International Fellowship Initiative (PIFI) for Visiting Scientists in 2017-18 and in 2019 (Grant No. 2017VCA0009). We appreciate detailed and constructive comments of Brad Peters and two anonymous reviewers as well as editorial handling by R. Walker, which helped us to improve the paper.

References

Abersteiner, A., Kamenetsky, V.S., Goemann, K., Golovin, A.V., Sharygin, I.S., Pearson, D.G., Kamenetsky, M. and Gornova, M.A. (2019) Polymineralic inclusions in kimberlite-hosted megacrysts: Implications for kimberlite melt evolution. Lithos 336-337, 310-325.

Abersteiner, A., Kamenetsky, V.S., Golovin, A.V., Kamenetsky, M. and Goemann, K. (2018) Was crustal contamination Involved in the formation of the serpentine-Free Udachnaya-East kimberlite? New insights into parental melts, liquidus assemblage and effects of alteration. Journal of Petrology 59, 1467-1492.

Agashev, A.M., Ionov, D.A., Pokhilenko, N.P., Golovin, A.V., Cherepanova, Y. and Sharygin, I.S. (2013) Metasomatism in lithospheric mantle roots: Constraints from whole-rock and mineral chemical composition of deformed peridotite xenoliths from kimberlite pipe Udachnaya. Lithos 160–161, 201-215.

Aulbach, S., Mungall, J.E. and Pearson, D.G. (2016) Distribution and Processing of Highly Siderophile Elements in Cratonic Mantle Lithosphere. Reviews in Mineralogy & Geochemistry 81, 239-304.

Bascou, J., Doucet, L.S., Saumet, S., Ionov, D.A., Ashchepkov, I.V. and Golovin, A.V. (2011) Seismic velocities, anisotropy and deformation in Siberian cratonic mantle: EBSD data on xenoliths from the Udachnaya kimberlite. Earth and Planetary Science Letters 304, 71-84.

Batanova, V.G., Thompson, J.M., Danyushevsky, L.V., Portnyagin, M.V., Garbe-Schönberg, D., Hauri, E., Kimura, J.-I., Chang, Q., Senda, R., Goemann, K., Chauvel, C., Campillo, S., Ionov, D.A. and Sobolev, A.V. (2019) New Olivine Reference Material for In Situ Microanalysis. Geostandards and Geoanalytical Research 43, 453-473.

Becker, H., Horan, M.F., Walker, R.J., Gao, S., Lorand, J.P. and Rudnick, R.L. (2006) Highly siderophile element composition of the Earth's primitive upper mantle: Constraints from new data on peridotite massifs and xenoliths. Geochimica et Cosmochimica Acta 70, 4528-4550.

Bernstein, S., Hanghoj, K., Kelemen, P. and Brooks, C. (2006) Ultra-depleted, shallow cratonic mantle beneath West Greenland: dunitic xenoliths from Ubekendt Ejland. Contributions to Mineralogy and Petrology 152, 335-347.

Boyd, F.R., Pokhilenko, N.P., Pearson, D.G., Mertzman, S.A., Sobolev, N.V. and Finger, L.W. (1997) Composition of the Siberian cratonic mantle: evidence from Udachnaya peridotite xenoliths. Contributions to Mineralogy and Petrology 128, 228-246.

Brenan, J.M. and Andrews, D. (2001) High-temperature stability of laurite and Ru-Os-Ir alloy and their role in PGE fractionation in mafic magmas. Can. Mineral. 39, 341-360.

Brey, G.P. and Köhler, T. (1990) Geothermobarometry in four-phase lherzolites II. New thermobarometers, and practical assessment of existing thermobarometers. Journal of Petrology 31, 1353-1378.

Burton, K.W., Schiano, P., Birck, J.-L., Allegre, C.J., Rehkämper, M., Halliday, A.N. and Dawson, J.B. (2000) The distribution and behaviour of rhenium and osmium amongst mantle minerals and the age of the lithospheric mantle beneath Tanzania. Earth Planet Sci Lett 183, 93-106.

Carlson, R.W. (2005) Application of the Pt–Re–Os isotopic systems to mantle geochemistry and geochronology. Lithos 82, 249-272.

Carlson, R.W., Pearson, D.G., Boyd, F.R., Shirey, S.B., Irvine, G., Menzies, A.H. and Gurney, J.J. (1999) Re-Os systematics of lithosphere peridotites: implications for lithosphere formation and preservation, in: Gurney, J.J., Gurney, J.L., Pascoe, M.D., Richardson, S.H. (Eds.), Proc. 7th Internatl. Kimberlite Conf. RedRoof Design, Cape Town, pp. 99-108.

Carlson, R.W., Pearson, D.G. and James, D.E. (2005) Physical, chemical, and chronological characteristics of continental mantle. Reviews of Geophysics 43, RG1001.

Condie, K.C. (2014) Growth of continental crust: a balance between preservation and recycling. Mineralogical Magazine 78, 623–637.

Doucet, L.S., Ionov, D.A. and Golovin, A.V. (2013) The origin of coarse garnet peridotites in cratonic lithosphere: new data on xenoliths from the Udachnaya kimberlite, central Siberia. Contributions to Mineralogy and Petrology 165, 1225-1242.

Doucet, L.S., Ionov, D.A. and Golovin, A.V. (2015) Paleoproterozoic formation age for the Siberian cratonic mantle: Hf and Nd isotope data on refractory peridotite xenoliths from the Udachnaya kimberlite. Chem Geol 391, 42-55.

Doucet, L.S., Ionov, D.A., Golovin, A.V. and Pokhilenko, N.P. (2012) Depth, degrees and tectonic settings of mantle melting during craton formation: inferences from major and trace element compositions of spinel harzburgite xenoliths from the Udachnaya kimberlite, central Siberia. Earth and Planetary Science Letters 359–360, 206-218.

Doucet, L.S., Mattielli, N., Ionov, D.A., Debouge, W. and Golovin, A.V. (2016) Zn isotopic heterogeneity in the mantle: A melting control? Earth and Planetary Science Letters 451, 232–240.

Doucet, L.S., Peslier, A.H., Ionov, D.A., Brandon, A.D., Golovin, A.V., Goncharov, A.G. and Ashchepkov, I.V. (2014) High water contents in the Siberian cratonic mantle linked to metasomatism: An FTIR study of Udachnaya peridotite xenoliths. Geochimica et Cosmochimica Acta 137, 159-187.

Golovin, A.V., Sharygin, I.S., Kamenetsky, V.S., Korsakov, A.V. and Yaxley, G.M. (2018) Alkali-

carbonate melts from the base of cratonic lithospheric mantle: Links to kimberlites. Chem Geol 483, 261-274.

Golovin, A.V., Sharygin, I.S., Korsakov, A.V., Kamenetsky, V.S. and Abersteiner, A. (2019) Can primitive kimberlite melts be alkali-carbonate liquids: Composition of the melt snapshots preserved in deepest mantle xenoliths. Journal of Raman Spectroscopy, 1-19, doi:10.1002/jrs.5701.

Goncharov, A.G., Ionov, D.A., Doucet, L.S. and Pokhilenko, L.N. (2012) Thermal state, oxygen fugacity and C-O-H fluid speciation in cratonic lithospheric mantle: new data on peridotite xenoliths from the Udachnaya kimberlite, Siberia. Earth and Planetary Science Letters 357-358, 99-110.

Herzberg, C. (2004) Geodynamic information in peridotite petrology. Journal of Petrology 45, 2507-2530.

Herzberg, C., Condie, K. and Korenaga, J. (2010) Thermal history of the Earth and its petrological expression. Earth and Planetary Science Letters 292, 79-88.

Herzberg, C. and Rudnick, R. (2012) Formation of cratonic lithosphere: An integrated thermal and petrological model. Lithos 149, 4-15.

Ionov, D.A. (1998) Trace element composition of mantle-derived carbonates and coexisting phases in peridotite xenoliths from alkali basalts. Journal of Petrology 39, 1931-1941.

Ionov, D.A., Ashchepkov, I. and Jagoutz, E. (2005) The provenance of fertile off-craton lithospheric mantle: Sr-Nd isotope and chemical composition of garnet and spinel peridotite xenoliths from Vitim, Siberia. Chem Geol 217, 41-75.

Ionov, D.A., Carlson, R.W., Doucet, L.S., Golovin, A.V. and Oleinikov, O.B. (2015a) The age and history of the lithospheric mantle of the Siberian craton: Re–Os and PGE study of peridotite xenoliths from the Obnazhennaya kimberlite. Earth and Planetary Science Letters 428, 108-119.

Ionov, D.A., Doucet, L.S. and Ashchepkov, I.V. (2010) Composition of the lithospheric mantle in the Siberian craton: new constraints from fresh peridotites in the Udachnaya-East kimberlite. Journal of Petrology 51, 2177-2210.

Ionov, D.A., Doucet, L.S., Carlson, R.W., Golovin, A.V. and Korsakov, A.V. (2015b) Post-Archean formation of the lithospheric mantle in the central Siberian craton: Re–Os and PGE study of peridotite xenoliths from the Udachnaya kimberlite. Geochimica et Cosmochimica Acta 165, 466-483.

Ionov, D.A., Doucet, L.S., Carlson, R.W., Golovin, A.V. and Oleinikov, O.B. (2018a) Lost in interpretation: Facts and misconceptions about the mantle of the Siberian craton. A comment on: "Composition of the lithospheric mantle in the northern part of Siberian craton: Constraints from peridotites in the Obnazhennaya kimberlite" by Sun et al. (2017). Lithos 314-315, 683-687.

Ionov, D.A., Doucet, L.S., Pogge von Strandmann, P.A.E., Golovin, A.V. and Korsakov, A.V. (2017) Links between deformation, chemical enrichments and Li-isotope compositions in the lithospheric mantle of the central Siberian craton. Chem Geol 475, 105-121.

Ionov, D.A., Doucet, L.S., Xu, Y., Golovin, A.V. and Oleinikov, O.B. (2018b) Reworking of Archean mantle in the NE Siberian craton by carbonatite and silicate melt metasomatism: Evidence

1067 from a carbonate-bearing, dunite-to-websterite xenolith suite from the Obnazhennaya kimberlite.
1068 Geochimica et Cosmochimica Acta 224, 132-153.
1069 Ionov, D.A. and Hofmann, A.W. (2007) Depth of formation of sub-continental off-craton
1070 peridotites. Earth and Planetary Science Letters 261, 620-634.
1071 Ionov, D.A., Savoyant, L. and Dupuy, C. (1992) Application of the ICP-MS technique to trace
1072 element analysis of peridotites and their minerals. Geostandards Newsletter 16, 311-315.
1073 Irvine, G.J., Pearson, D.G., Kjarsgaard, B.A., Carlson, R.W., Kopylova, M.G. and Dreibus, G.
1074 (2003) A Re-Os isotope and PGE study of kimberlite-derived peridotite xenoliths from Somerset
1075 Island and a comparison to the Slave and Kaapvaal cratons. Lithos 71, 461-488.
1076 Ishikawa, A., Senda, R., Suzuki, K., Dale, C.W. and Meisel, T. (2014) Re-evaluating digestion
1077 methods for highly siderophile element and 187Os isotope analysis: Evidence from geological
1078 reference materials. Chem Geol 384, 27-46.
1079 Jean, M.M., Taylor, L.A., Howarth, G.H., Peslier, A.H., Fedele, L., Bodnar, R.J., Guan, Y.,
1080 Doucet, L.S., Ionov, D.A., Logvinova, A.M., Golovin, A.V. and Sobolev, N.V. (2016) Olivine
1081 inclusions in Siberian diamonds and mantle xenoliths: Contrasting water and trace-element contents.
1082 Lithos 265, 31-41.
1083 Kamenetsky, V.S., Golovin, A.V., Maas, R., Giuliani, A., Kamenetsky, M.B. and Weiss, Y. (2014)
1084 Towards a new model for kimberlite petrogenesis: Evidence from unaltered kimberlites and mantle
1085 minerals. Earth-Science Reviews 139, 145-167.
1086 Kamenetsky, V.S., Kamenetsky, M.B., Golovin, A.V., Sharygin, V.V. and Maas, R. (2012)
1087 Ultrafresh salty kimberlite of the Udachnaya–East pipe (Yakutia, Russia): A petrological oddity or
1088 fortuitous discovery? Lithos 152, 173-186.
1089 Kamenetsky, V.S., Kamenetsky, M.B., Sobolev, A.V., Golovin, A.V., Demouchy, S., Faure, K.,
1090 Sharygin, V.V. and Kuzmin, D.V. (2008) Olivine in the Udachnaya-East kimberlite (Yakutia, Russia):
1091 Types, compositions and origins. Journal of Petrology 49, 823-839.
1092 Kang, J.-T., Ionov, D.A., Liu, F., Zhang, C.-L., Golovin, A.V., Qin, L.-P., Zhang, Z.-F. and Huang,
1093 F. (2017) Calcium isotopic fractionation in mantle peridotites by melting and metasomatism and Ca
1094 isotope composition of the Bulk Silicate Earth. Earth and Planetary Science Letters 474, 128-137.
1095 Kelemen, P.B., Joyce, D.B., Webster, J.D. and Holloway, J.R. (1990) Reaction between ultramafic
1096 rocks and fractionating basaltic magma. Experimental investigation of reaction between olivine
1097 tholeiite and harzburgite at 1150-1050°C and 5 Kb. J. Petrol. 31, 99-134.
1098 Kinny, P.D., Griffin, B.J., Heaman, L.M., Brakhfogel, F.F. and Spetsius, Z.V. (1997) SHRIMP U-
1099 Pb ages of perovskite from Yakutian kimberlites. Geologiya i Geofizika 38, 91-99 (in Russian).
1100 Kitayama, Y., Thomassot, E., Galy, A., Golovin, A., Korsakov, A., d'Eyrames, E., Assayag, N.,
1101 Bouden, N. and Ionov, D. (2017) Co-magmatic sulfides and sulfates in the Udachnaya-East pipe
1102 (Siberia): A record of the redox state and isotopic composition of sulfur in kimberlites and their
1103 mantle sources. Chem Geol 455, 315-330.

Li, J., Liang, X.-R., Xu, J.-F., Suzuki, K. and Dong, Y.-H. (2010) Simplified technique for the measurements of Re-Os isotope by multicollector inductively coupled plasma mass spectrometry (MC-ICP-MS). Geochemical Journal 44, 73-80.

Liu, J., Brin, L.E., Graham Pearson, D., Bretschneider, L., Luguet, A., van Acken, D., Kjarsgaard, B., Riches, A. and Mišković, A. (2018) Diamondiferous Paleoproterozoic mantle roots beneath Arctic Canada: A study of mantle xenoliths from Parry Peninsula and Central Victoria Island. Geochimica et Cosmochimica Acta 239, 284-311.

Liu, J., Riches, A.J.V., Pearson, D.G., Luo, Y., Kienlen, B., Kjarsgaard, B.A., Stachel, T. and Armstrong, J.P. (2016) Age and evolution of the deep continental root beneath the central Rae craton, northern Canada. Precambrian Research 272, 168-184.

Luguet, A., Behrens, M., Pearson, D.G., König, S. and Herwartz, D. (2015) Significance of the whole rock Re–Os ages in cryptically and modally metasomatised cratonic peridotites: Constraints from HSE–Se–Te systematics. Geochimica et Cosmochimica Acta 164, 441-463.

McDonough, W.F. and Sun, S.-s. (1995) The composition of the Earth. Chem Geol 120, 223-253.

Meisel, T., Walker, R.J., Irving, A.J. and Lorand, J.-P. (2001) Osmium isotopic compositions of mantle xenoliths: a global perspective. Geochim. Cosmochim. Acta 65, 1311-1323.

Meisel, T., Walker, R.J. and Morgan, J.W. (1996) The osmium isotopic composition of the Earth's primitive upper mantle. Nature 383, 517-520.

Moyen, J.-F., Paquette, J.L., Ionov, D.A., Gannoun, A., Korsakov, A.V., Golovin, A.V. and Moine, B.N. (2017) Paleoproterozoic rejuvenation and replacement of Archaean lithosphere: Evidence from zircon U-Pb dating and Hf isotopes in crustal xenoliths at Udachnaya, Siberian craton. Earth Planet Sci Lett 457, 149-159.

Nickel, K.G. and Green, D.H. (1985) Empirical geothermobarometry for garnet peridotites and implications for the nature of the lithosphere, kimberlites and diamonds. Earth and Planetary Science Letters 73, 158-170.

Nimis, P. and Grütter, H. (2010) Internally consistent geothermometers for garnet peridotites and pyroxenites. Contributions to Mineralogy and Petrology 159, 411-427.

Nimis, P. and Taylor, W.R. (2000) Single clinopyroxene thermobarometry for garnet peridotites. Part I. Calibration and testing of a Cr-in-Cpx barometer and an enstatite-in-Cpx thermometer. Contributions to Mineralogy and Petrology 139, 541-554.

Palme, H. and O'Neill, H.S.C. (2014) Cosmochemical Estimates of Mantle Composition, in: Carlson, R.W. (Ed.), Treatise on Geochemistry (Second Edition). Elsevier, Oxford, pp. 1-39.

Paquette, J.L., Ionov, D.A., Agashev, A.M., Gannoun, A. and Nikolenko, E.I. (2017) Age, provenance and Precambrian evolution of the Anabar shield from U-Pb and Lu-Hf isotope data on detrital zircons, and the history of the northern and central Siberian craton. Precambrian Research 301, 134-144.

Pearson, D.G. (1999) The age of continental roots. Lithos 48, 171-194.

Pearson, D.G., Carlson, R.W., Shirey, S.B., Boyd, F.R. and Nixon, P.H. (1995a) Stabilisation of Archaen lithospheric mantle: A Re-Os isotope study of peridotite xenoliths from the Kaapvaal craton. Earth and Planetary Science Letters 134, 341-357.

Pearson, D.G., Irvine, G.J., Ionov, D.A., Boyd, F.R. and Dreibus, G.E. (2004) Re-Os isotope systematics and platinum group element fractionation during mantle melt extraction: a study of massif and xenolith peridotite suites. Chem Geol 208, 29-59.

Pearson, D.G., Shirey, S.B., Carlson, R.W., Boyd, F.R., Pokhilenko, N.P. and Shimizu, N. (1995b) Re-Os, Sm-Nd, and Rb-Sr isotope evidence for thick Archaean lithospheric mantle beneath the Siberian craton modified by multistage metasomatism. Geochimica et Cosmochimica Acta 59, 959-977.

Pearson, D.G., Snyder, G.A., Shirey, S.B., Taylor, L.A., Carlson, R.W. and Sobolev, N.V. (1995c) Archaean Re-Os age for Siberian eclogites and constraints on Archaean tectonics. Nature 374, 711-713.

Pearson, D.G. and Wittig, N. (2008) Formation of Archaean continental lithosphere and its diamonds: the root of the problem. J. Geol. Soc. London 165, 895-914.

Pernet-Fisher, J.F., Barry, P.H., Day, J.M.D., Pearson, D.G., Woodland, S., Agashev, A.M., Pokhilenko, L.N. and Pokhilenko, N.P. (2019) Heterogeneous kimberlite metasomatism revealed from a combined He-Os isotope study of Siberian megacrystalline dunite xenoliths. Geochimica et Cosmochimica Acta 266, 220-236.

Pernet-Fisher, J.F., Howarth, G.H., Pearson, D.G., Woodland, S., Barry, P.H., Pokhilenko, N.P., Pokhilenko, L.N., Agashev, A.M. and Taylor, L.A. (2015) Plume impingement on the Siberian SCLM: Evidence from Re–Os isotope systematics. Lithos 218–219, 141-154.

Pokhilenko, N.P., Pearson, D.G., Boyd, F.R. and Sobolev, N.V. (1991) Megacrystalline dunites: sources of Siberian diamonds. Carnegie Inst. Washington Yearbook 90, 11-18.

Pokhilenko, N.P., Sobolev, N.V., Boyd, F.R., Pearson, D.G. and Shimizu, N. (1993) Megacrystalline pyrope peridotites in the lithosphere of the Siberian platform: mineralogy, geochemical peculiarities and the problem of their origin. Russian Geology and Geophysics 34, 56-67.

Pollack, H.N. and Chapman, D.S. (1977) On the regional variation of heat flow, geotherms and lithospheric thickness. Tectonophysics 38, 279-296.

Priyatkina, N., Khudoley, A.K., Collins, W.J., Kuznetsov, N.B. and Huang, H.-Q. (2016) Detrital zircon record of Meso- and Neoproterozoic sedimentary basins in northern part of the Siberian Craton: Characterizing buried crust of the basement. Precambrian Research 285, 21-38.

Reisberg, L. and Lorand, J.P. (1995) Longevity of sub-continental mantle lithosphere from osmium isotope systematics in orogenic peridotite massifs. Nature 376, 159-162.

Reisberg, L., Zhi, X., Lorand, J.-P., Wagner, C., Peng, Z. and Zimmermann, C. (2005) Re–Os and S systematics of spinel peridotite xenoliths from east central China: Evidence for contrasting effects of melt percolation. Earth Planet Sci Lett 239, 286-308.

Rosen, O.M. (2002) Siberian craton - a fragment of a Paleoproterozoic supercontinent. Russian Journal of Earth Sciences 4, 103-119.

Rudnick, R.L. and Walker, R.J. (2009) Interpreting ages from Re–Os isotopes in peridotites Lithos 112, Supplement 2, 1083-1095.

Servali, A. and Korenaga, J. (2018) Oceanic origin of continental mantle lithosphere. Geology 46, 1047-1050.

Shimizu, N., Pokhilenko, N.P., Boyd, F.R. and Pearson, D.G. (1997) Geochemical characteristics of mantle xenoiliths from the Udachnaya kimberlite pipe. Russian Geology and Geophysics 38, 205-217.

Shirey, S.B. and Walker, R.J. (1998) The Re-Os isotope system in cosmochemistry and high-temperature geochemistry. Annu. Rev. Earth Planet. Sci. 26, 423-500.

Smoliar, M.I., Walker, R.J. and Morgan, J.W. (1996) Re–Os ages of group IIA, IIIA, IVA, and IVB iron meteorites. Science 271, 1099– 1102.

Sobolev, N.V., Logvinova, A.M., Zedgenizov, D.A., Pokhilenko, N.P., Malygina, E.V., Kuzmin, D.V. and Sobolev, A.V. (2009) Petrogenetic significance of minor elements in olivines from diamonds and peridotite xenoliths from kimberlites of Yakutia Lithos 112, 701-713.

Sobolev, N.V., Pokhilenko, N.V. and Efimova, E.S. (1984) Diamond-bearing peridotite xenoliths in kimberlite and the problem of the origin of diamonds. Russ. Geol. Geofys. 25, 63-80.

Spetsius, Z.V. and Serenko, V.P. (1990) Composition of the continental upper mantle and lower crust beneath the Siberian Platform. Nauka, Moscow.

Streckeisen, A. (1976) To each plutonic rock its proper name. Earth Sci. Rev. 12, 1-33.

Takazawa, E., Frey, F.A., Shimizu, N. and Obata, M. (2000) Whole rock compositional variations in an upper mantle peridotite (Horoman, Hokkaido, Japan): Are they consistent with a partial melting process. Geochimica et Cosmochimica Acta 64, 695-716.

Taylor, W.R. (1998) An experimental test of some geothermometer and geobarometer formulations for upper mantle peridotites with application to the thermobarometry of fertile Iherzolite and garnet websterite. Neues Jahrbuch fur Mineralogie-Abhandlungen 172, 381-408.

Walker, R.J., Carlson, R.W., Shirey, S.B. and Boyd, F.R. (1989) Os, Sr, Nd, and Pb isotope systematics of southern African peridotite xenoliths: Implications for the chemical evolution of subcontinental mantle. Geochim. Cosmochim. Acta 53, 1583-1595.

Walker, R.J., Horan, M.F., Morgan, J.W., Becker, H., Grossman, J.N. and Rubin, A.E. (2002a) Comparative ^{187}Re-^{187}Os systematics of chondrites - Implications regarding early solar system processes. Geochim. Cosmochim. Acta 66, 4187-4201.

Walker, R.J., Prichard, H.M., Ishiwatari, A. and Pimentel, M. (2002b) The osmium isotopic composition of convecting upper mantle deduced from ophiolite chromites. Geochim. Cosmochim. Acta 66, 329-345.

Walter, M.J. (1999) Melting residues of fertile peridotite and the origin of cratonic lithosphere, in:

Fei, Y., Bertka, C.M., Mysen, B.O. (Eds.), Mantle Petrology: Field Observations and High-Pressure Experimentation. Spec. Publ. Geochem. Soc. No. 6. Geochemical Society, Houston, pp. 225-239.

Walter, M.J. (2003) Melt extraction and compositional variability in mantle lithosphere, in: Carlson, R.W. (Ed.), Treatise on Geochemistry. Vol. 2. The Mantle and Core. Elsevier, Amsterdam, pp. 363-394.

Wang, H., van Hunen, J. and Pearson, D.G. (2018) Making Archean cratonic roots by lateral compression: A two-stage thickening and stabilization model. Tectonophysics 746, 562-571.

Wiggers de Vries, D.F., Pearson, D.G., Bulanova, G.P., Smelov, A.P., Pavlushin, A.D. and Davies, G.R. (2013) Re–Os dating of sulphide inclusions zonally distributed in single Yakutian diamonds: Evidence for multiple episodes of Proterozoic formation and protracted timescales of diamond growth. Geochimica et Cosmochimica Acta 120, 363-394.

Wittig, N., Pearson, D.G., Baker, J.A., Duggen, S. and Hoernle, K. (2010a) A major element, PGE and Re-Os isotope study of Middle Atlas (Morocco) peridotite xenoliths: Evidence for coupled introduction of metasomatic sulphides and clinopyroxene. Lithos 115, 15-26.

Wittig, N., Pearson, D.G., Webb, M., Ottley, C.J., Irvine, G.J., Kopylova, M., Jensen, S.M. and Nowell, G.M. (2008) Origin of cratonic lithospheric mantle roots: A geochemical study of peridotites from the North Atlantic Craton, West Greenland. Earth and Planetary Science Letters 274, 24-33.

Wittig, N., Webb, M., Pearson, D.G., Dale, C.W., Ottley, C.J., Hutchison, M., Jensen, S.M. and Luguet, A. (2010b) Formation of the North Atlantic Craton: Timing and mechanisms constrained from Re-Os isotope and PGE data of peridotite xenoliths from S.W. Greenland. Chem Geol 276, 166-187.

Xia, J., Qin, L., Shen, J., Carlson, R.W., Ionov, D.A. and Mock, T.D. (2017) Chromium isotope heterogeneity in the mantle. Earth and Planetary Science Letters 464, 103-115.

Zhang, J., Li, J., Long, X., Sun, S., Yin, L. and Dai, M. (2017) Rhenium-Osmium isotope measurements of geological reference material BIR-1a: Evaluation of homogeneity and implications for method validation and quality control. Geostandards and Geoanalytical Research 41, 649-658.

Ziberna, L., Nimis, P., Kuzmin, D.V. and Malkovets, V.G. (2016) Error sources in single-clinopyroxene thermobarometry and a mantle geotherm for the Novinka kimberlite, Yakutia. American Mineralogist 101, 2222-2232.

Figure captions

Fig. 1. Photomicrographs of Udachnaya mantle xenoliths in transmitted plane-polarized light. Abbreviations: Ol, olivine; Op, orthopyroxene; Cp, clinopyroxene; Gar, garnet; Sp, spinel. A-B: Olivine megacrysts contain inclusions of Op, Sp (B) and Gar. C-F: coarse dunites (Ol ≤1 cm; ≤8% Op); pyroxene, garnet and spinel grains are usually small and interstitial (E-F), but

some samples contain Op-Sp±Cp intergrowths (C; breakdown products of garnet or high-T Op) and patches enriched in Gar (D; metasomatic products). G-H: low-opx harzburgites (11–21% Op) with grain size ranging from medium (G) to coarse (H).

Fig. 2. Co-variation plots for modal mineral abundances and $Mg\#_{WR}$ $(Mg/(Mg+Fe)_{mol}$ in whole-rock samples). Abbreviations: Dun, dunite; Hzb, harzburgite; Opx (Op), orthopyroxene; Cpx, clinopyroxene; Gar, garnet; r^2, linear correlation coefficient. (A) Olivine and Opx abundances show a robust ($r^2 = 0.94$) linear correlation for all xenolith types, except megacrysts with high modal garnet. For simplicity, megacrystalline dunite Uv83-13 and olivine megacrysts are shown as "megacrysts". (B-F) Abundances of garnet and Cpx show the same variation range (from zero to 5–6%) in coarse dunites and low-Opx harzburgites and are not correlated (low r^2) with modal olivine or $Mg\#_{WR}$. The absence of robust correlations of modal abundances with $Mg\#_{WR}$ indicate that they are not caused by melt extraction events, and are likely due to metasomatism.

Fig. 3. Co-variation plots for major and minor oxides (wt. %) and Mg# $(Mg/(Mg+Fe)_{mol})$ in whole-rock (WR) xenoliths in this study. The concentrations of oxides hosted mainly by the low-abundance garnet, cpx and oxides (Al_2O_3, CaO, Cr_2O_3) are not correlated with Mg# and show the same range for coarse dunites and harzburgites; the harzburgites can be distinguished with $(Mg/Si)_{mol}$ ratios (B) and the concentrations of MgO, NiO and Na_2O (e, f) that depend on olivine/opx ratios. Olivine megacrysts and megacrystalline dunite Uv83-13 show lower average concentrations of CaO and Al_2O_3 and higher MgO than coarse dunites.

Fig. 4. Co-variation plots of Al_2O_3 vs. FeO (A) and SiO_2 (B) in whole-rock (WR) xenoliths in this study (wt. %). Abbreviations are same as in Fig. 2. Also shown are: primitive mantle (PM) after McDonough and Sun (1995), and the fields of cratonic peridotite xenoliths (Doucet et al., 2013), fertile off-craton peridotite xenoliths from Vitim and Tariat in central Asia (Ionov et al., 2005; Ionov and Hofmann, 2007), and Horoman massif peridotites that are

residues of low-pressure melting of fertile mantle (Takazawa et al., 2000). Colored lines are experimental melting residues of batch (blue) and polybaric (red) fractional melting of fertile mantle (Herzberg, 2004). Thick dashed blue lines show 45% of isobaric batch melting; thick dashed red lines show 38% of polybaric fractional melting.

Fig. 5. Co-variation plots for major oxides, Mg# ($Mg/(Mg+Fe)_{mol}$) and Cr# ($Cr/(Cr+Al)_{mol}$) in minerals and whole-rocks, and mineral abundances. The Mg# for silicates are the highest in olivine and the lowest in garnet (A). The xenoliths containing much low-Mg# garnet and/or ilmenite plot off the linear $Mg\#_{Ol}$ vs. $Mg\#_{WR}$ correlation (B). The abundance of garnet is proportional to WR Al_2O_3 (C). Literature data for Cr# in coarse garnet peridotites from Udachnaya in (D) are from Doucet et al. (2013); samples that plot to the right from the linear $Cr\#_{WR}$ vs. $Cr\#_{Gar}$ correlation (defined by the earlier work) contain Cr-spinel.

Fig. 6. A plot of pressure vs. temperature (P-T) estimates for peridotites in this study (Table 1). Gar Meg are garnet-bearing megacrysts. Pressure for garnet-free peridotites (smaller symbols) is fixed at 3.5 GPa for harzburgites and 4 GPa for dunites. Dunites and olivine megacrysts are equilibrated in a broad P range (hence, do not come from a specific depth level in the lithosphere) and plot between the $35mW/m^2$ and $40mW/m^2$ model conductive geotherms (Pollack and Chapman, 1977). Also shown are graphite/diamond (G/D) stability boundary and mantle adiabats for Tp=1250°C and 1300°C.

Fig. 7. Primitive mantle-normalized (McDonough and Sun, 1995) patterns for the REE (left column) and lithophile trace elements (right column) in whole-rock (WR) samples in this study. Blue lines are olivine megacrysts, red lines are coarse dunites, continuous grey lines are low-opx harzburgites, dashed grey lines are high-opx harzburgites. Dark-grey fields are for Udachnaya kimberlites (Kamenetsky et al., 2012). Light-grey fields in plots for coarse dunites outline the data for harzburgites.

Fig. 8. (a) Primitive mantle-normalized (McDonough and Sun, 1995) REE patterns for

garnets in this study (blue lines, olivine megacrysts; red lines, coarse dunites; grey lines are low-opx harzburgites, dashed grey line is garnet 565-10 low in LREE-MREE. Fields in (B-C) outline the data for olivine megacrysts.

Fig. 9. Primitive mantle-normalized patterns for PGE (Becker et al., 2006) and Re (Meisel et al., 2001) in olivine megacrysts (A), coarse dunites (B) and low-opx harzburgites (C) in this study. Dashed lines in (B) and (C) are for peridotites with low Os (<0.04 ppb) and/or high Re (≥0.3 ppb).

Fig. 10. Plots of $^{187}Os/^{188}Os$ vs. $^{187}Re/^{188}Os$ for samples in this study. (A) Taken together (except for sheared dunite 48-12), the 23 xenoliths define a positive linear correlation with a slope corresponding to an age of 0.37 ± 0.12 Ga (2σ), identical to the eruption age of host kimberlite, and initial $^{187}Os/^{188}Os = 0.1127 \pm 0.0026$. Sample 48-12 with aberrantly high $^{187}Os/^{188}Os$ (0.44) and $^{187}Re/^{188}Os$ (40.7) values plots close to the extension of this isochron trend. (B) Harzburgites show higher $^{187}Os/^{188}Os$ ratios than dunites and megacrysts in the subset of xenoliths that show no Os depletions and/or Re enrichments. The four olivine megacrysts and megacrystalline dunite 83-13 define an 'isochron' (green line) with an apparent 2.7 ± 1.2 Ga age and an 0.1069 ± 0.0017 initial, but the uncertainty of this estimate is too high, and the data are too few, to argue that these samples have a common origin or differ in age from coarse dunites.

Fig. 11. Plots of olivine (A) and orthopyroxene (B) abundances vs. model Re-depletion Os isotope ages (T_{RD}) for appropriate xenoliths in this study (excepting those with ≤0.04 ppb Os). The T_{RD} ages are calculated relative to primitive mantle (PM): $^{187}Os/^{188}Os = 0.1296$ (Meisel et al., 2001), $^{187}Re/^{188}Os = 0.4353$ (Becker et al., 2006) and $\lambda^{187}Re = 1.666 \times 10^{-11}$ a^{-1} (Smoliar et al., 1996). Re-enriched samples (Re/Os close to or higher than in PM, hence uncertain T_{RD}) are shown as empty symbols. Continuous straight lines show linear correlations of the robust T_{RD} values (samples with low Re/Os) with modal abundances for individual rock types: (i)

harzburgites (triangles) and (ii) dunites (red circles) grouped with olivine megacrysts (green circles). Thin dashed lines show linear correlations of the T_{RD} with modal abundances for all the xenoliths. The T_{RD} seem to be correlated with modal olivine and opx when all the xenoliths are treated as a single statistical sample (correlation factors r^2 ~0.6–0.7). However, these seeming correlations are artefacts of combining distinct xenolith types in a single statistical population because the T_{RD} show opposite correlation trends for individual rock types (or no correlation, with r^2 close to zero, if samples with high Re/Os are included). Overall, the plots reflect bimodal age distribution: Paleoproterozoic for harzburgites and mainly Archean for dunites and olivine megacrysts. This observation, together with the lack of correlation of the modal abundances with Mg# (Fig. 2 D-F) confirms that the T_{RD} are not controlled by gradual differences in modal and chemical compositions or melting degrees.

Fig. 12. Cumulative probability distribution (Gaussian plots) for Re-depletion Os isotope ages (T_{RD}) of mantle xenoliths from the Siberian craton (A) and for U-Pb ages of zircons from its Precambrian crustal basement (B). **(**A) The T_{RD} ages for xenoliths in this study (except Os-depleted and/or Re-enriched samples): red, coarse dunites; green, olivine megacrysts; blue, low-opx harzburgites. Also shown are literature data for peridotite xenoliths from Udachnaya (Ionov et al., 2015b) and Obnazhennaya (Ionov et al., 2015a), and for high-Mg# olivine megacrysts from Udachnaya (Pearson et al., 1995b; Pernet-Fisher et al., 2019) re-calculated with the PM BSE model (dotted line). The lines are obtained by summing the probability distributions of a suite of data with normally-distributed errors. T_{RD} uncertainties (standard deviation, σ) are calculated using the error transfer function; the peak widths are scaled by the uncertainty of each analysis. The T_{RD} uncertainties of 2σ are used for the Udachnaya data and of 4σ for the Obnazhennaya data to smooth the plots. (B) Combined U-Pb age data for zircons from crustal xenoliths (n = 487) in the Udachnaya kimberlite (Moyen et al., 2017), detrital zircons from the Anabar shield (n = 479) north of Udachnaya (Paquette et al., 2017) and from

1349 nearby Meso- and Neoproterozoic sediments (n = 814) (Priyatkina et al., 2016).

1350

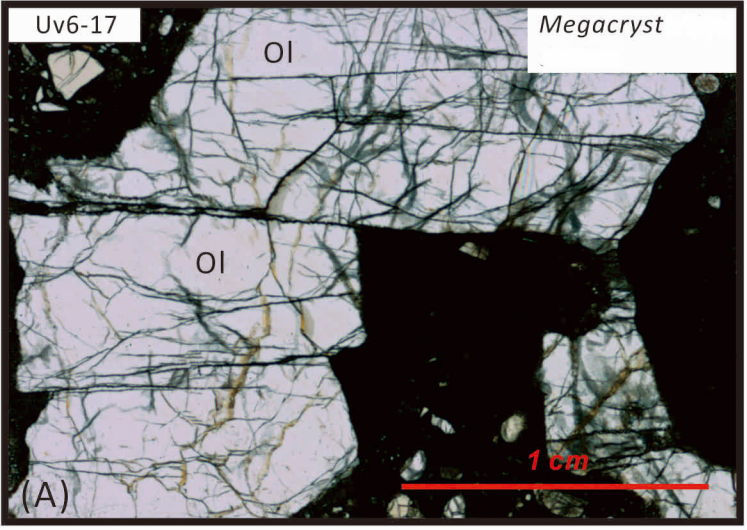
Uv6-17
Megacryst
Ol
Ol
1 cm
(A)

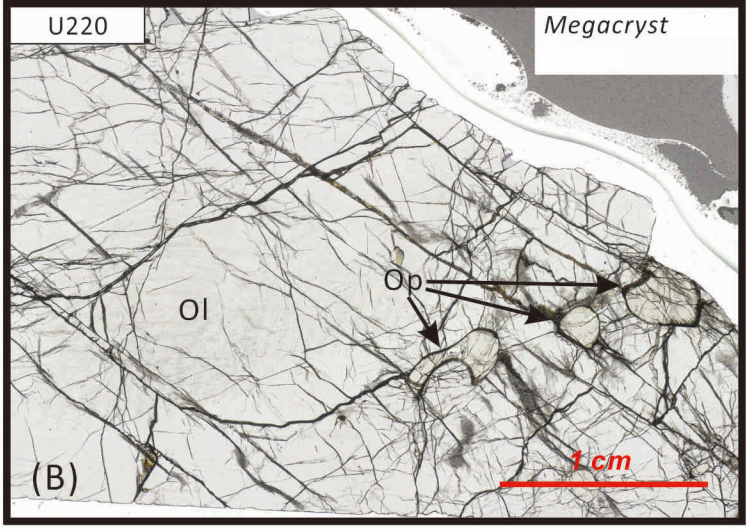
U220
Megacryst
Op
Ol
1 cm
(B)

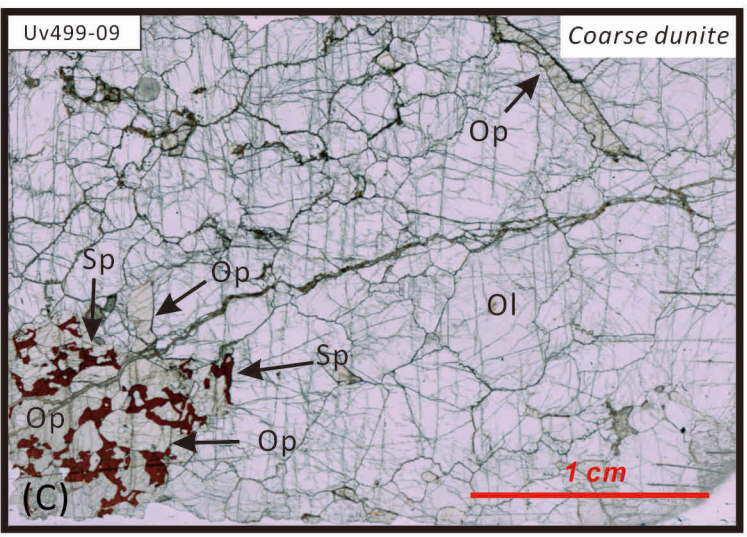
Uv499-09
Coarse dunite
Op
Sp
Op
Ol
Sp
Op
Op
1 cm
(C)

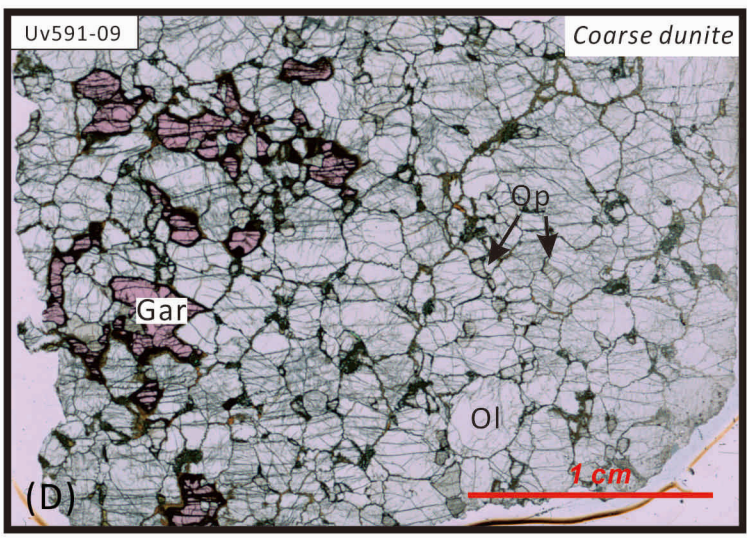
Uv591-09
Coarse dunite
Op
Gar
Ol
1 cm
(D)

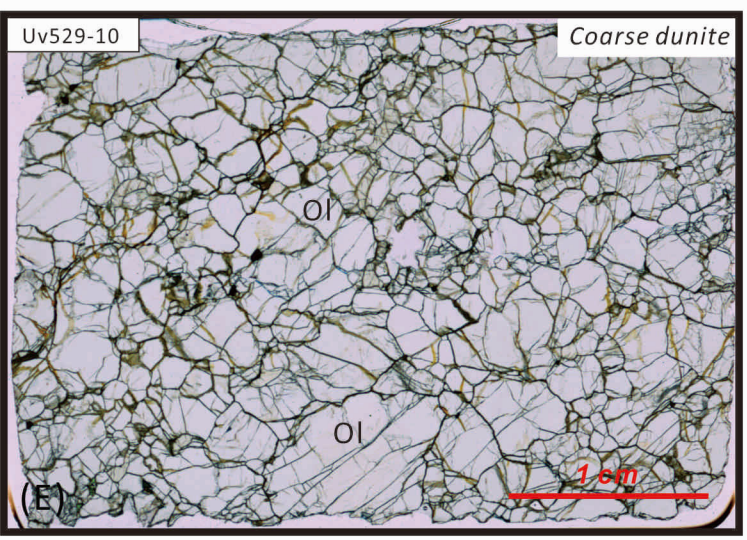
Uv529-10
Coarse dunite
Ol
Ol
1 cm
(E)

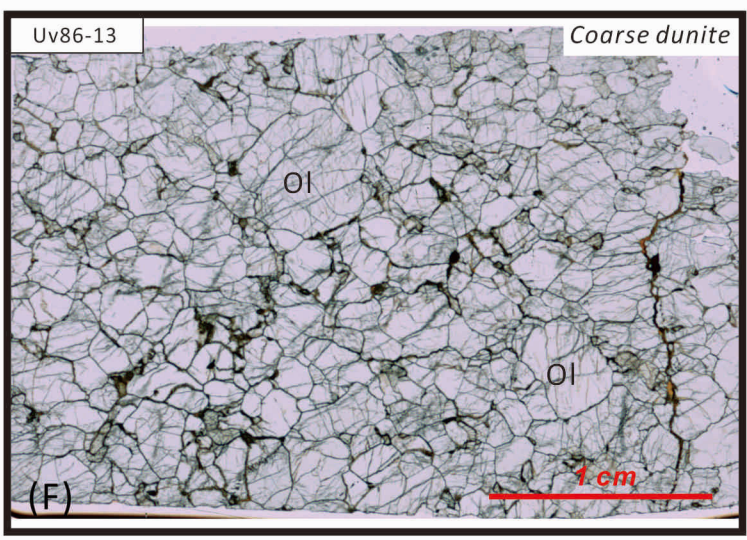
Uv86-13
Coarse dunite
Ol
Ol
1 cm
(F)

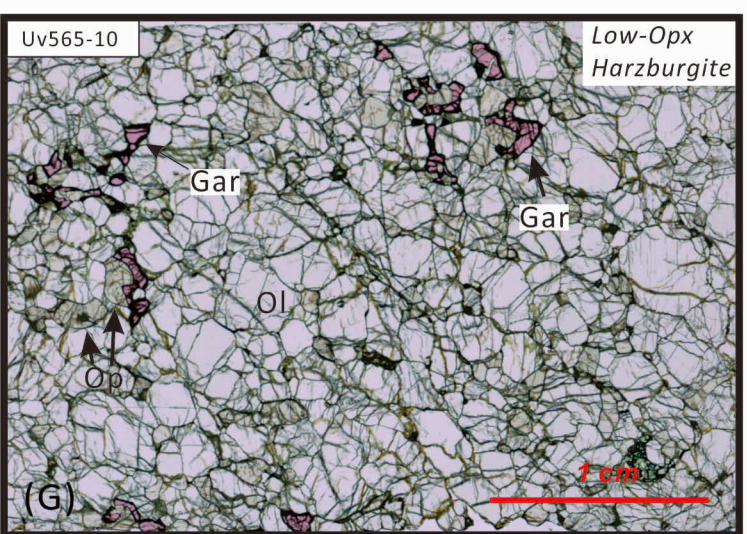
Uv565-10
Low-Opx
Harzburgite
Gar
Gar
Ol
Op
1 cm
(G)

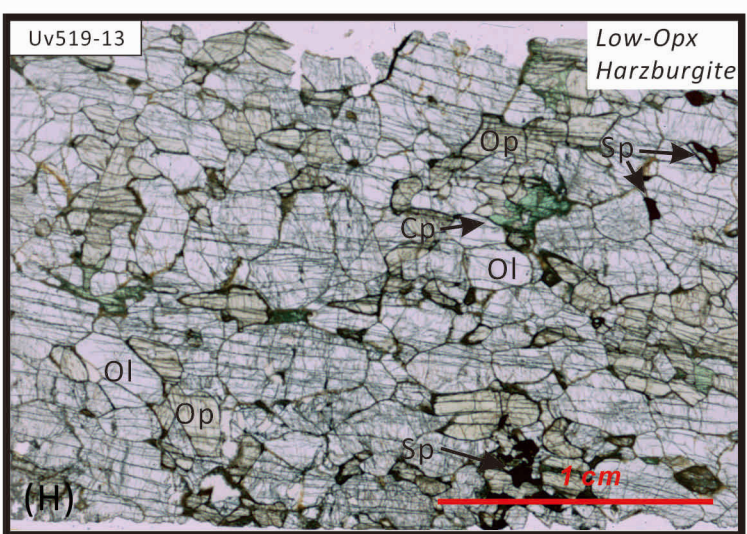
Uv519-13
Low-Opx
Harzburgite
Op
Sp
Cp
Ol
Ol
Op
Sp
1 cm
(H)

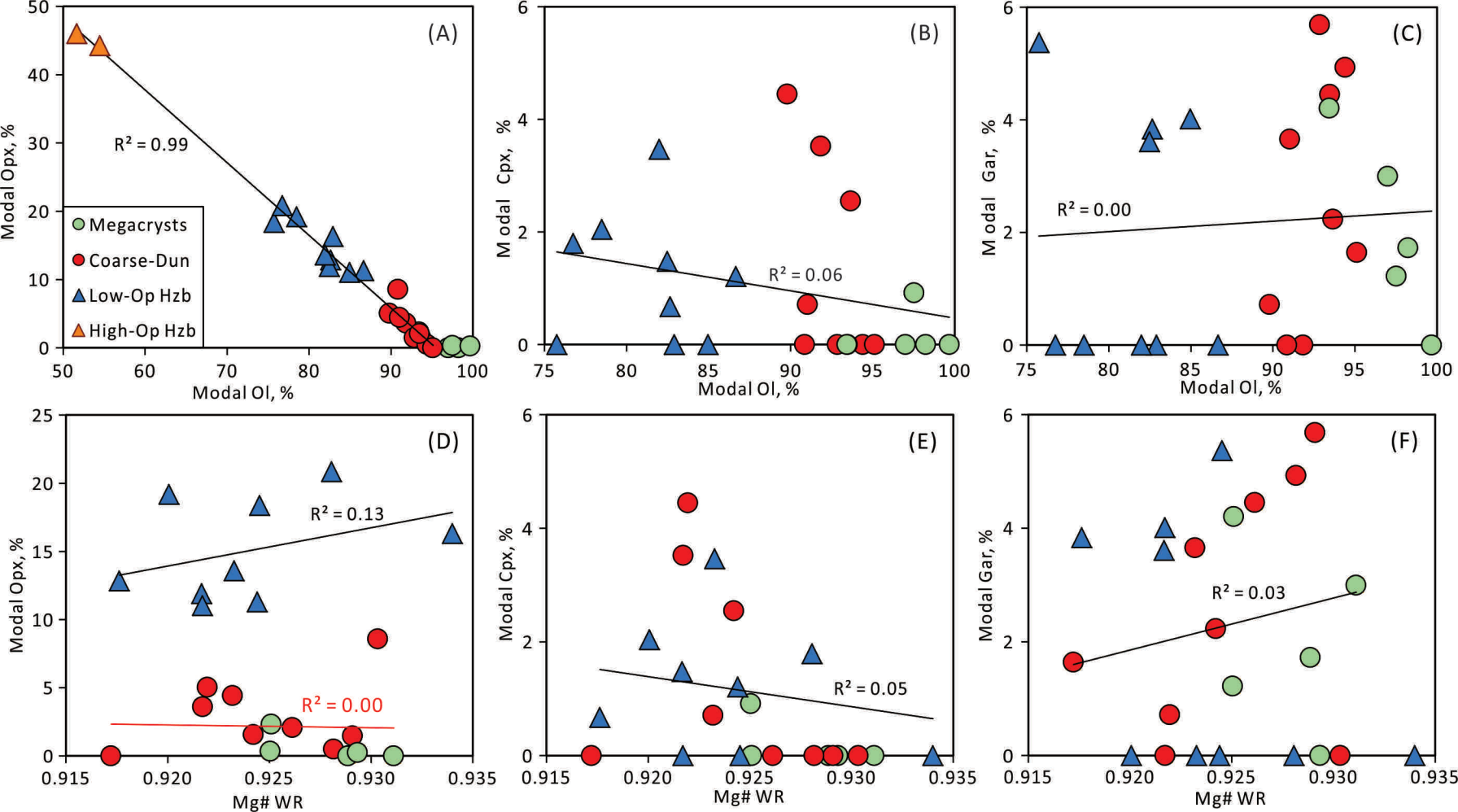
(A)
Modal Opx, %
Modal Ol, %
R² = 0.99
Megacrysts
Coarse-Dun
Low-Op Hzb
High-Op Hzb
(B)
Modal Cpx, %
Modal Ol, %
R² = 0.06
(C)
Modal Gar, %
Modal Ol, %
R² = 0.00
(D)
Modal Opx, %
Mg# WR
R² = 0.13
R² = 0.00
(E)
Modal Cpx, %
Mg# WR
R² = 0.05
(F)
Modal Gar, %
Mg# WR
R² = 0.03

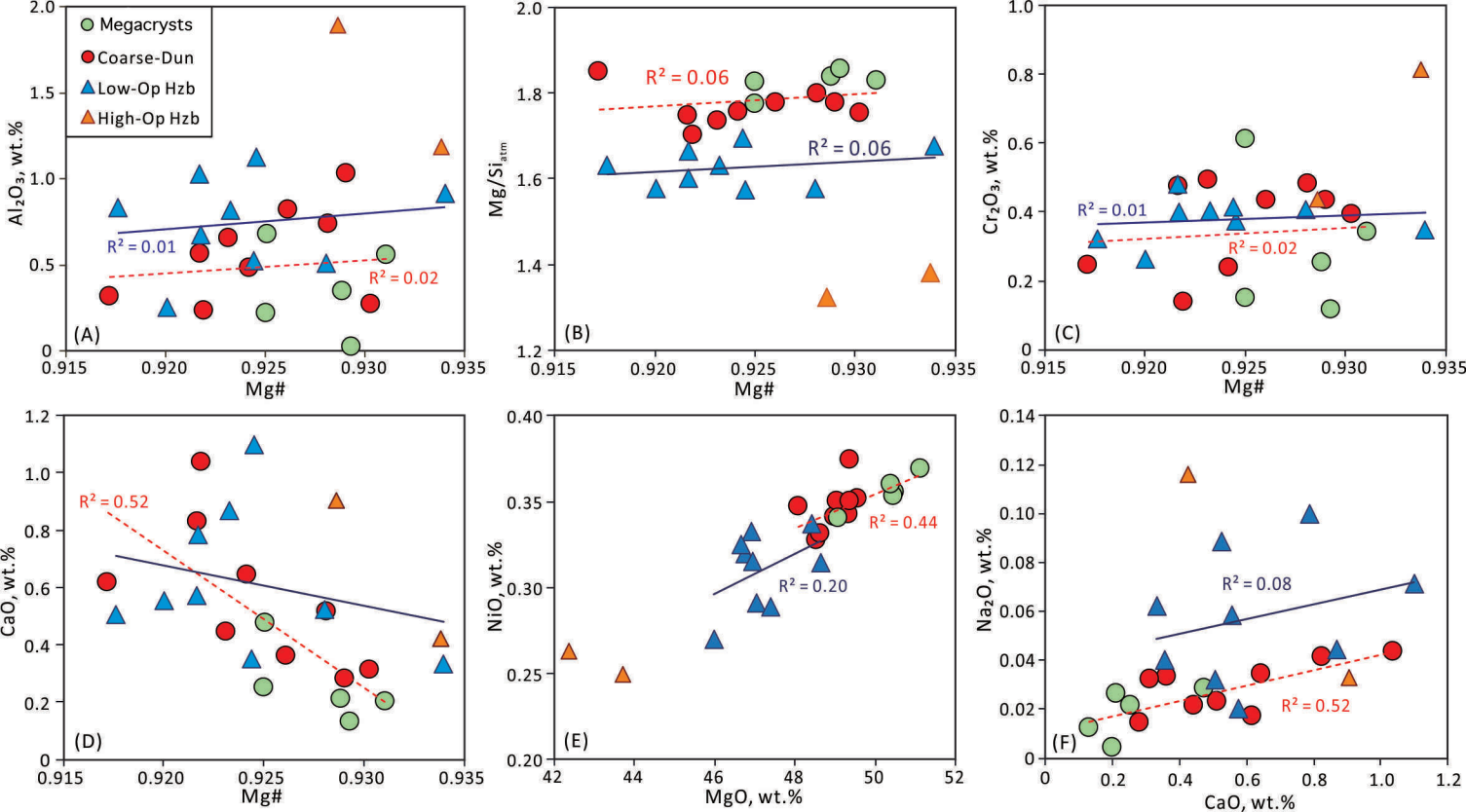
Megacrysts
Coarse-Dun
Low-Op Hzb
High-Op Hzb
(A)
Al2O3, wt.%
Mg#
R² = 0.01
R² = 0.02
(B)
Mg/Siatm
Mg#
R² = 0.06
R² = 0.06
(C)
Cr2O3, wt.%
Mg#
R² = 0.01
R² = 0.02
(D)
CaO, wt.%
Mg#
R² = 0.52
(E)
NiO, wt.%
MgO, wt.%
R² = 0.44
R² = 0.20
(F)
Na2O, wt.%
CaO, wt.%
R² = 0.08
R² = 0.52

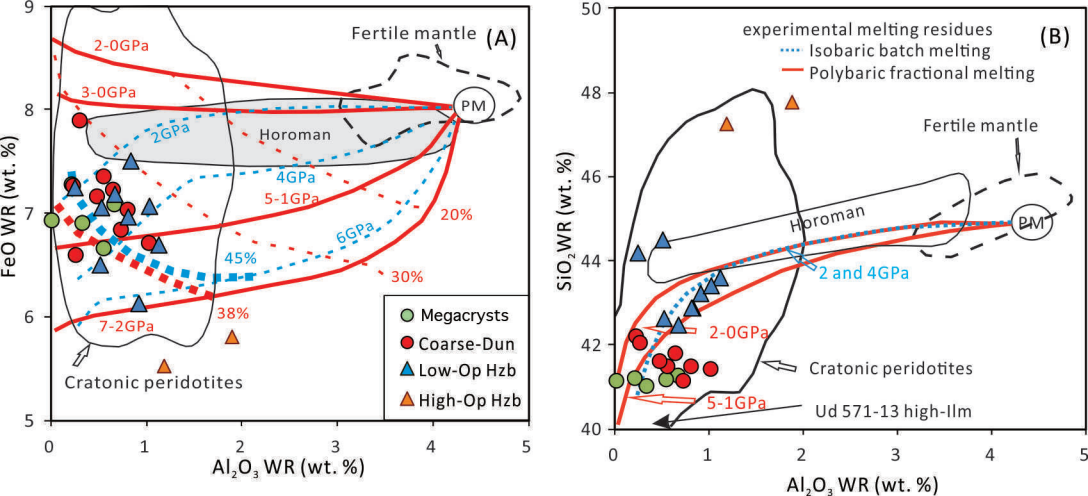
(A)
Fertile mantle
PM
2-0GPa
3-0GPa
2GPa
Horoman
4GPa
5-1GPa
6GPa
20%
45%
30%
38%
7-2GPa
Cratonic peridotites
Megacrysts
Coarse-Dun
Low-Op Hzb
High-Op Hzb
FeO WR (wt. %)
Al2O3 WR (wt. %)
(B)
experimental melting residues
Isobaric batch melting
Polybaric fractional melting
Fertile mantle
PM
Horoman
2 and 4GPa
2-0GPa
Cratonic peridotites
5-1GPa
Ud 571-13 high-Ilm
SiO2 WR (wt. %)
Al2O3 WR (wt. %)

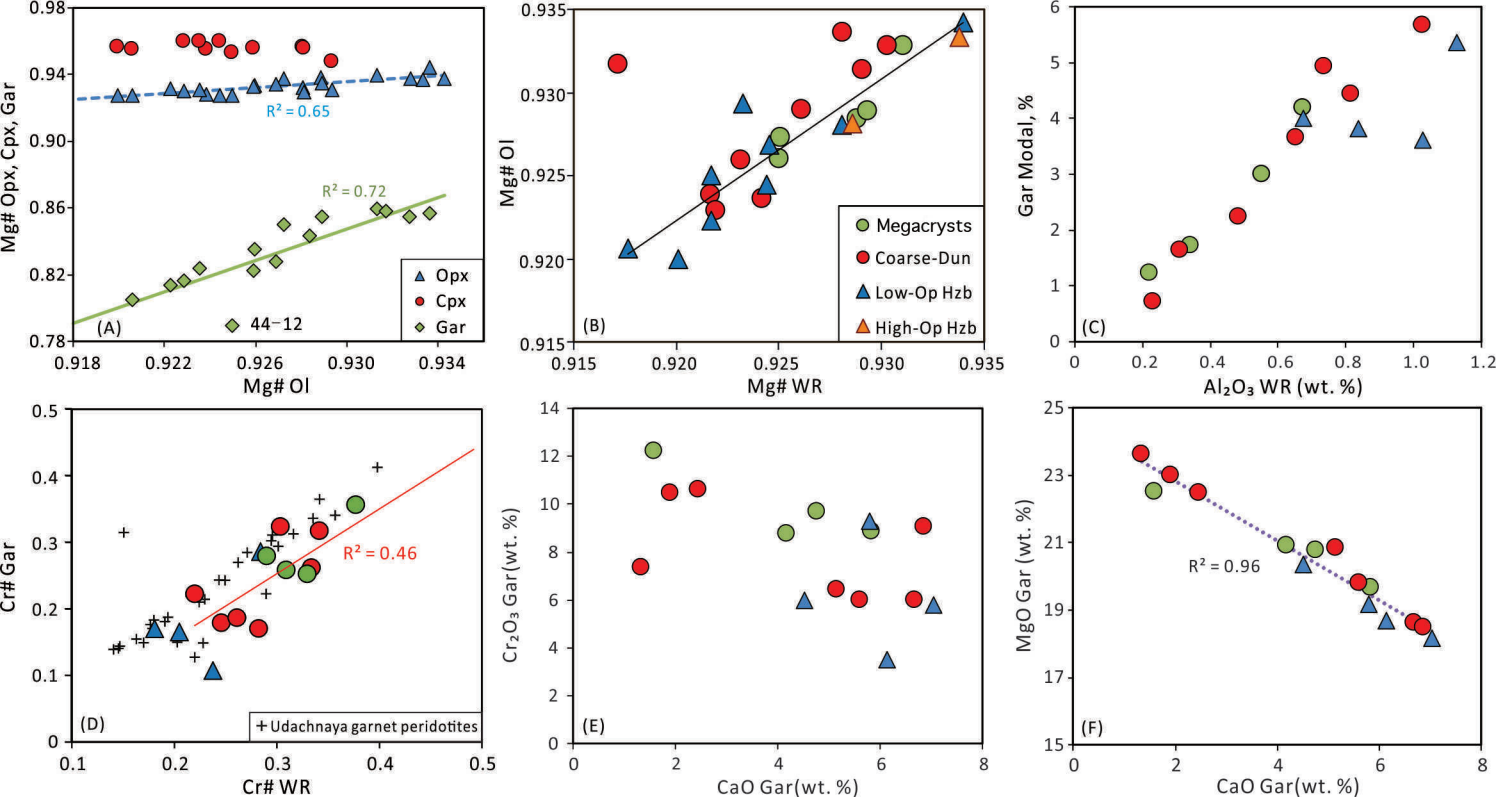
Mg# Opx, Cpx, Gar
Mg# Ol
R² = 0.65
R² = 0.72
(A)
44−12
Opx
Cpx
Gar
Mg# Ol
Mg# WR
(B)
Megacrysts
Coarse-Dun
Low-Op Hzb
High-Op Hzb
Gar Modal, %
Al2O3 WR (wt. %)
(C)
Cr# Gar
Cr# WR
R² = 0.46
(D)
Udachnaya garnet peridotites
Cr2O3 Gar(wt. %)
CaO Gar(wt. %)
(E)
MgO Gar (wt. %)
R² = 0.96
(F)
CaO Gar(wt. %)

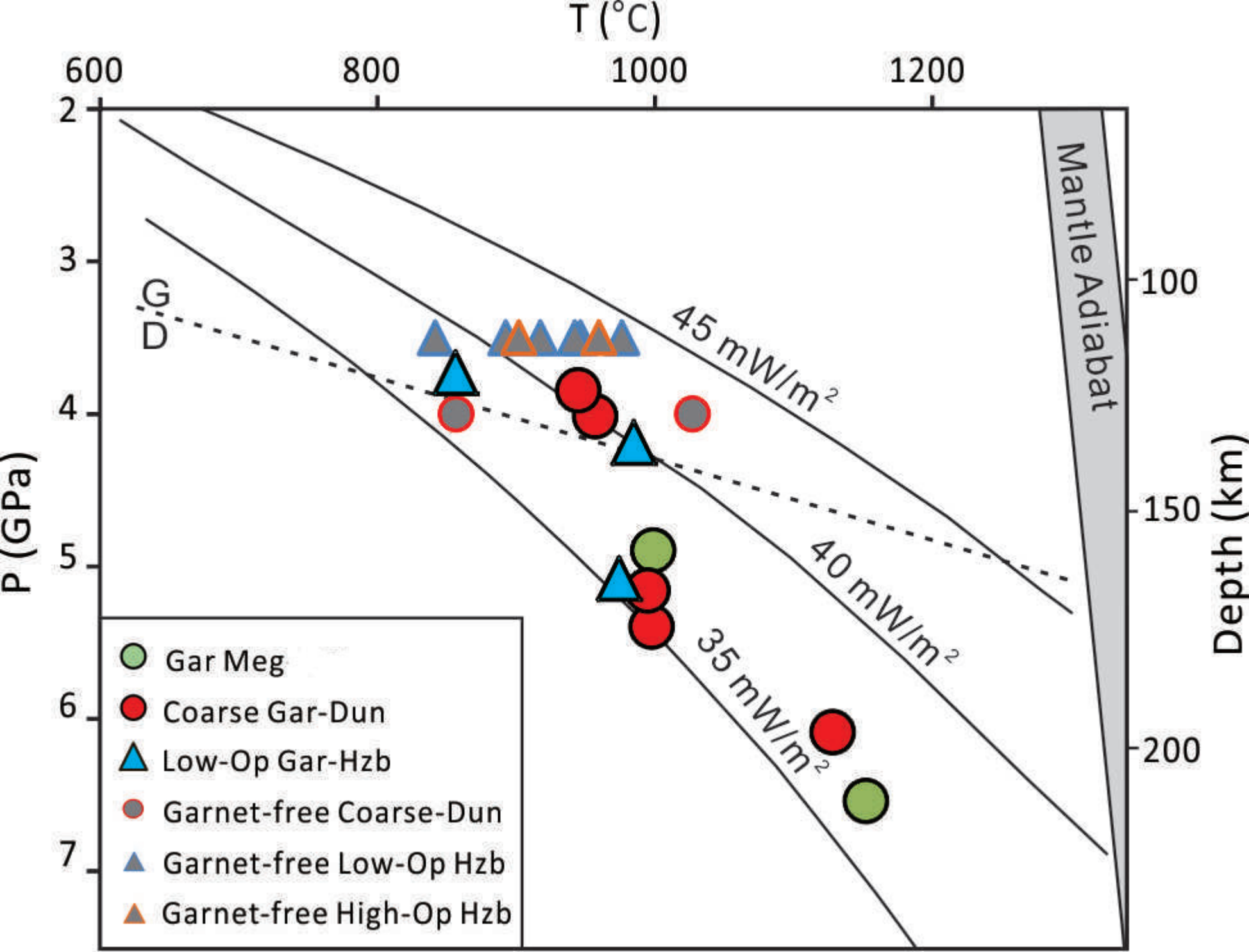
T (°C)
600
800
1000
1200
2
3
4
5
6
7
P (GPa)
100
150
200
Depth (km)
G
D
45 mW/m²
40 mW/m²
35 mW/m²
Mantle Adiabat
Gar Meg
Coarse Gar-Dun
Low-Op Gar-Hzb
Garnet-free Coarse-Dun
Garnet-free Low-Op Hzb
Garnet-free High-Op Hzb

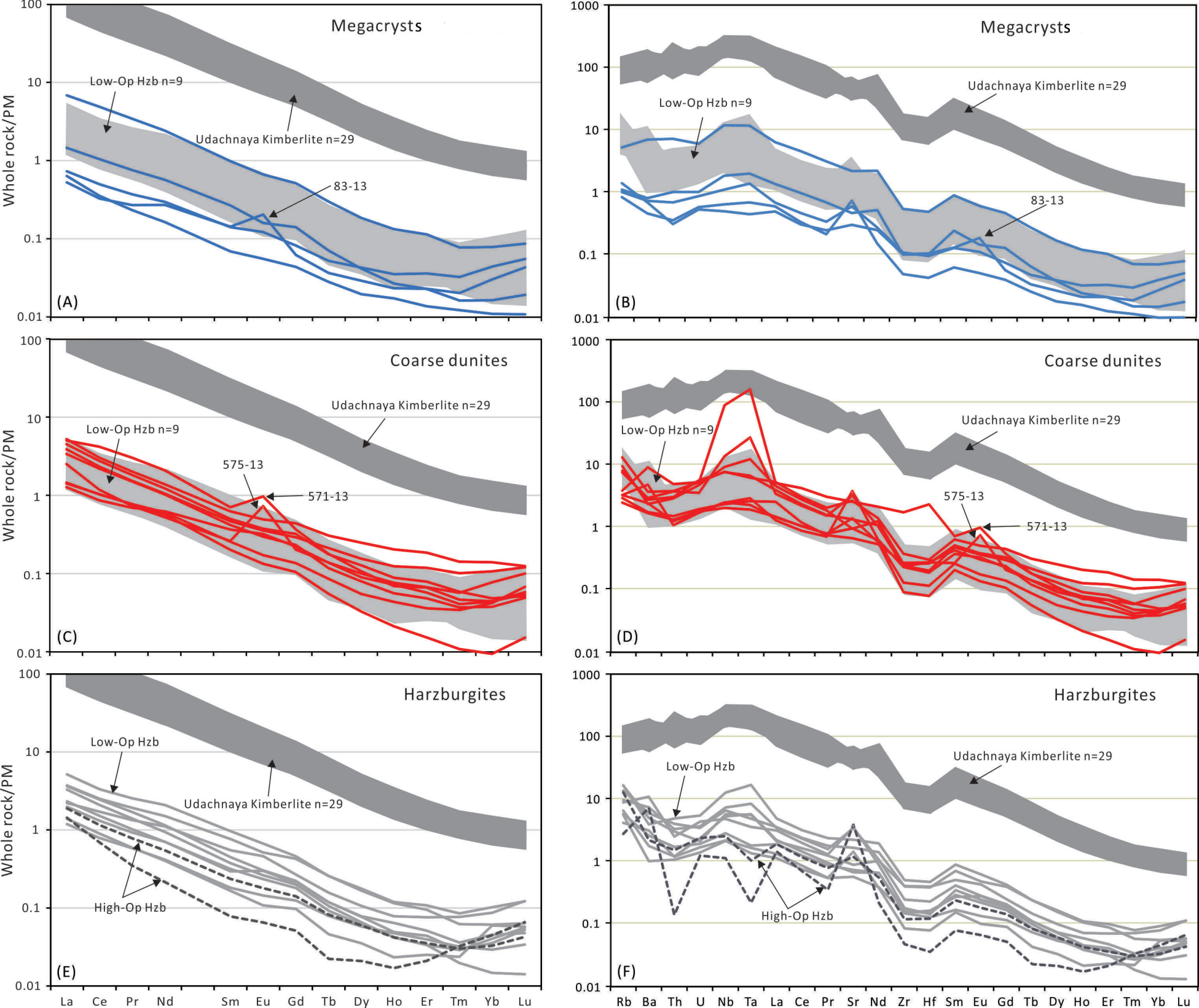
Megacrysts
Low-Op Hzb n=9
Udachnaya Kimberlite n=29
83-13
(A)
Megacrysts
Udachnaya Kimberlite n=29
Low-Op Hzb n=9
83-13
(B)
Coarse dunites
Udachnaya Kimberlite n=29
Low-Op Hzb n=9
575-13
571-13
(C)
Coarse dunites
Udachnaya Kimberlite n=29
Low-Op Hzb n=9
575-13
571-13
(D)
Harzburgites
Low-Op Hzb
Udachnaya Kimberlite n=29
High-Op Hzb
(E)
Harzburgites
Udachnaya Kimberlite n=29
Low-Op Hzb
High-Op Hzb
(F)
Whole rock/PM
La Ce Pr Nd Sm Eu Gd Tb Dy Ho Er Tm Yb Lu
Rb Ba Th U Nb Ta La Ce Pr Sr Nd Zr Hf Sm Eu Gd Tb Dy Ho Er Tm Yb Lu

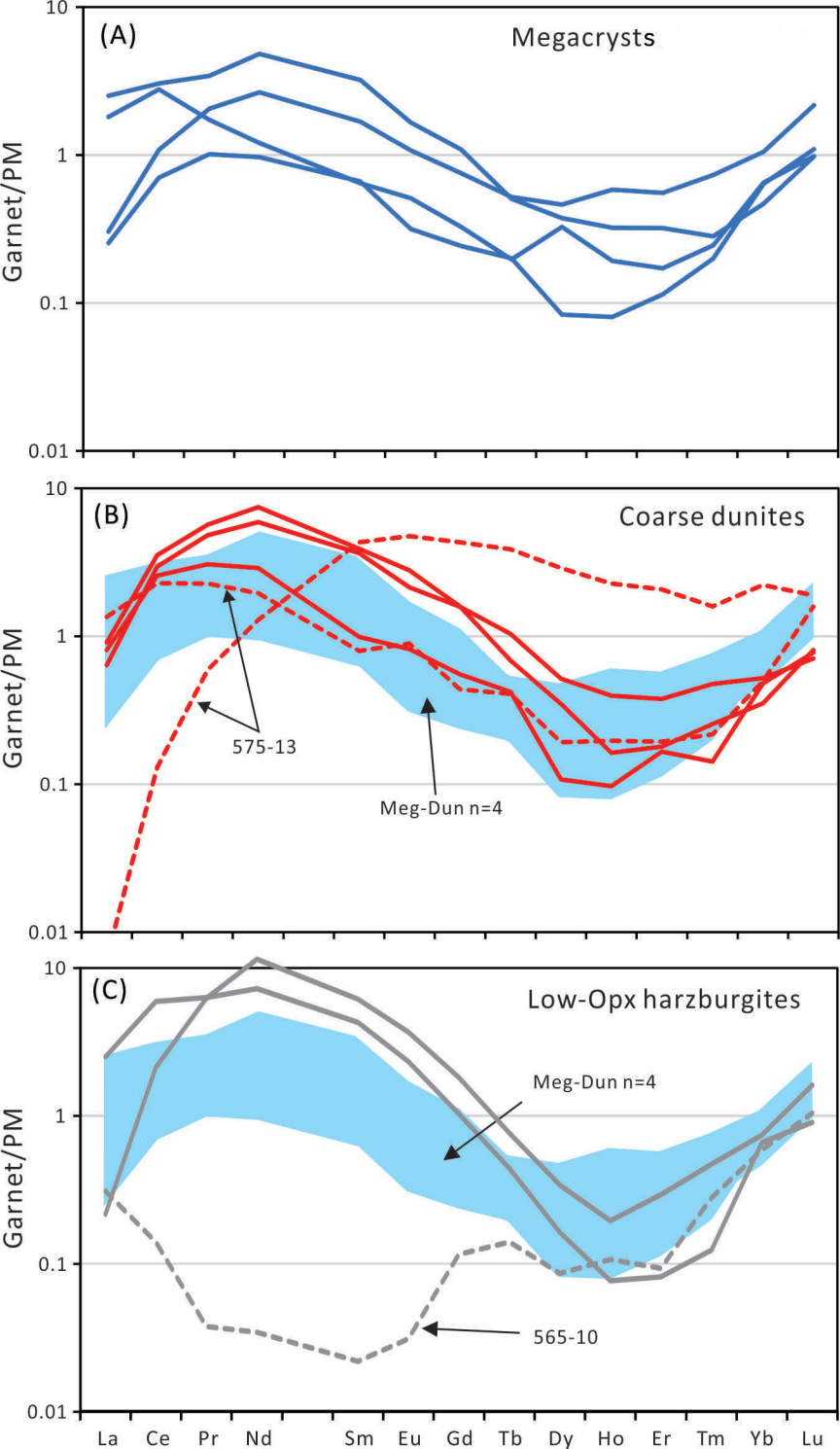
(A)
Megacrysts
Garnet/PM
10
1
0.1
0.01
(B)
Coarse dunites
575-13
Meg-Dun n=4
(C)
Low-Opx harzburgites
Meg-Dun n=4
565-10
La
Ce
Pr
Nd
Sm
Eu
Gd
Tb
Dy
Ho
Er
Tm
Yb
Lu

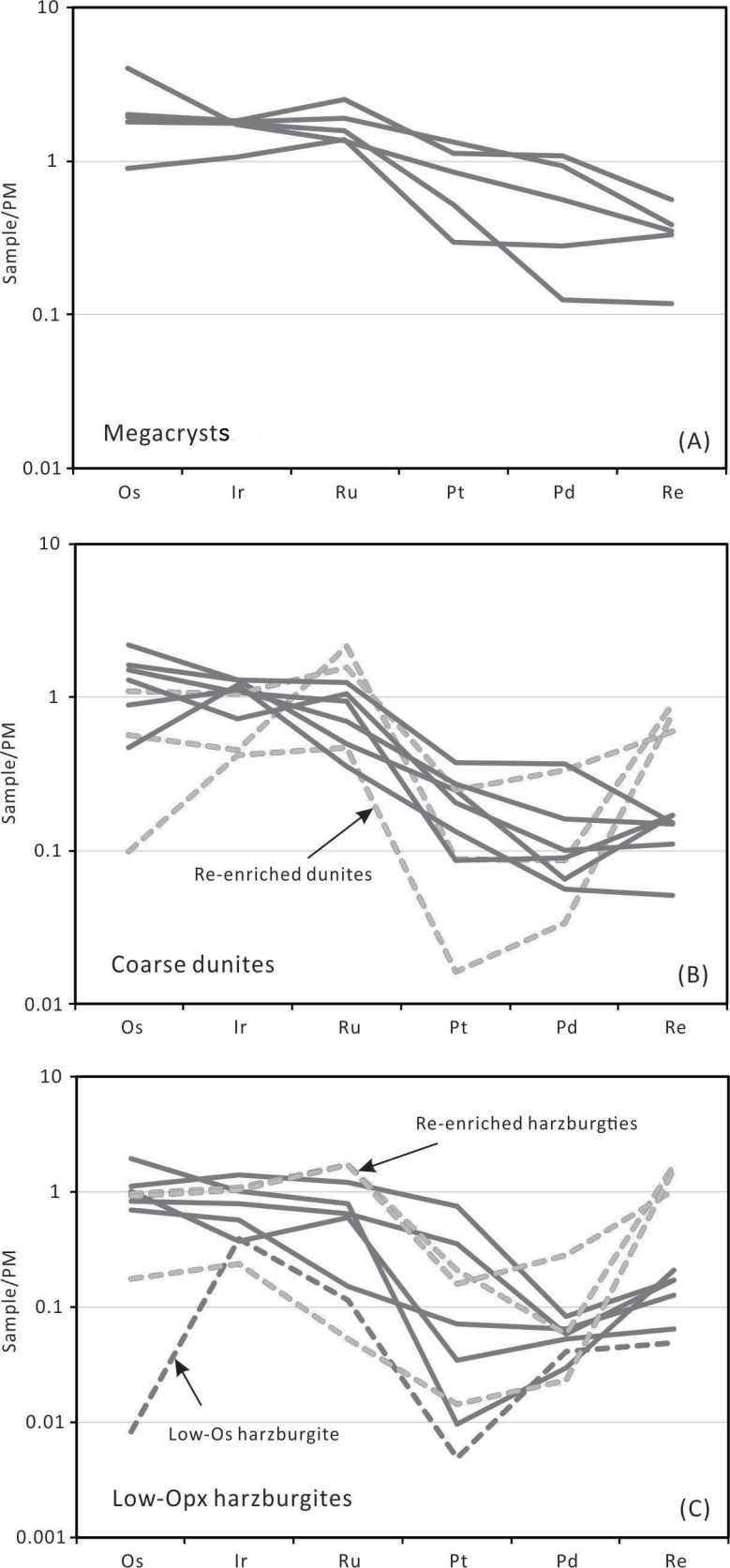
10
1
0.1
0.01
Sample/PM
Megacrysts
(A)
Os
Ir
Ru
Pt
Pd
Re
10
1
0.1
0.01
Sample/PM
Re-enriched dunites
Coarse dunites
(B)
Os
Ir
Ru
Pt
Pd
Re
10
1
0.1
0.01
0.001
Sample/PM
Re-enriched harzburgties
Low-Os harzburgite
Low-Opx harzburgites
(C)
Os
Ir
Ru
Pt
Pd
Re

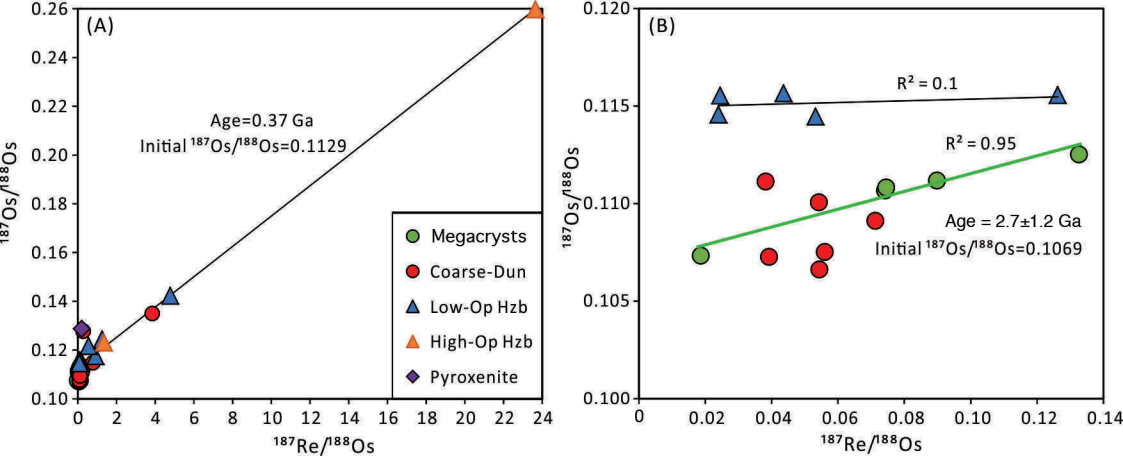
(A)
Age=0.37 Ga
Initial 187Os/188Os=0.1129
Megacrysts
Coarse-Dun
Low-Op Hzb
High-Op Hzb
Pyroxenite
187Os/188Os
187Re/188Os
(B)
R2 = 0.1
R2 = 0.95
Age = 2.7±1.2 Ga
Initial 187Os/188Os=0.1069
187Os/188Os
187Re/188Os

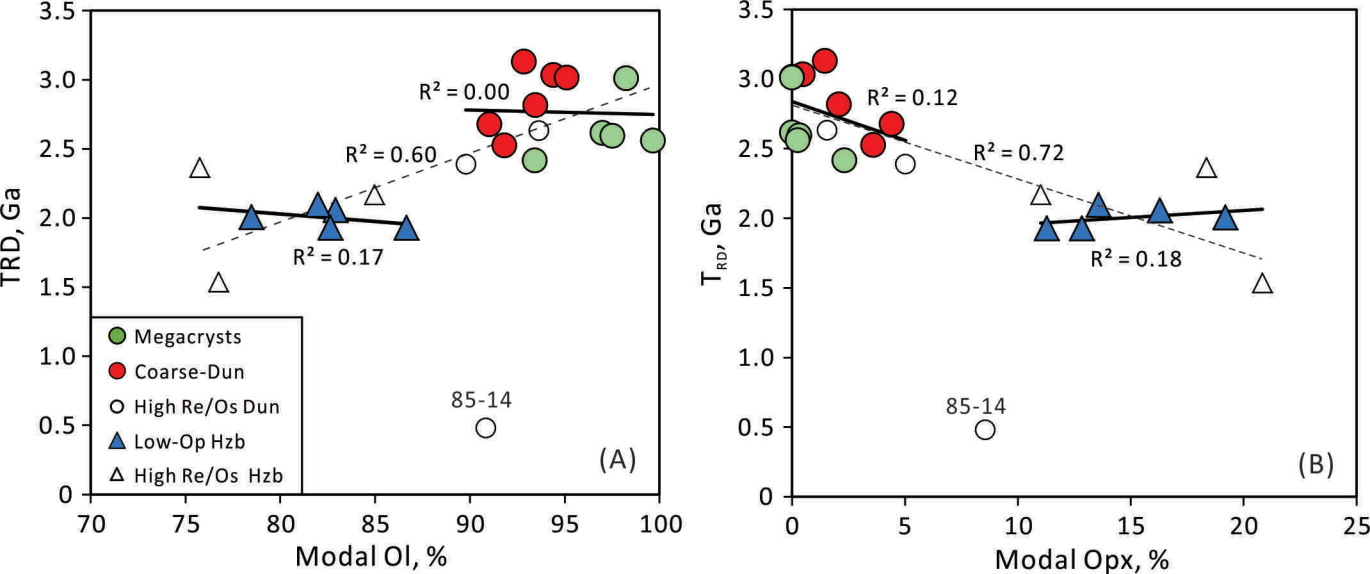
TRD, Ga
Modal Ol, %
R² = 0.00
R² = 0.60
R² = 0.17
Megacrysts
Coarse-Dun
High Re/Os Dun
Low-Op Hzb
High Re/Os Hzb
85-14
(A)
T_RD, Ga
Modal Opx, %
R² = 0.12
R² = 0.72
R² = 0.18
85-14
(B)

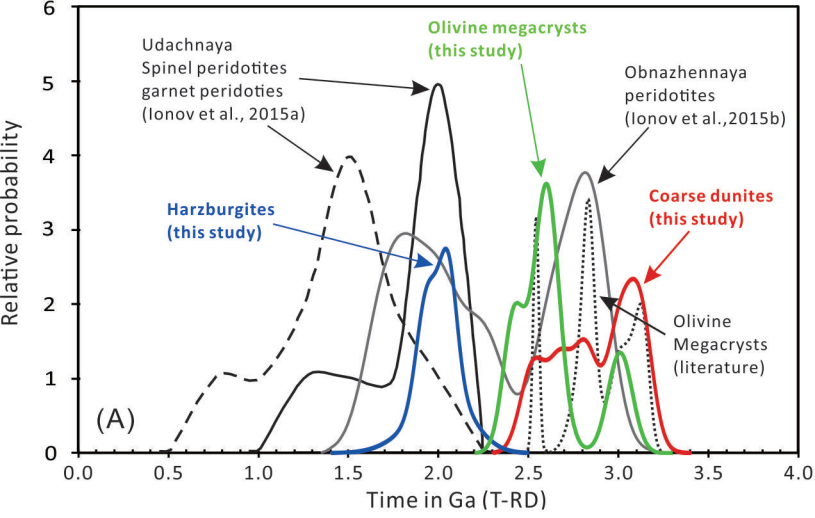
Udachnaya
Spinel peridotites
garnet peridoties
(Ionov et al., 2015a)
Olivine megacrysts
(this study)
Obnazhennaya
peridotites
(Ionov et al.,2015b)
Harzburgites
(this study)
Coarse dunites
(this study)
Olivine
Megacrysts
(literature)
(A)
Relative probability
Time in Ga (T-RD)

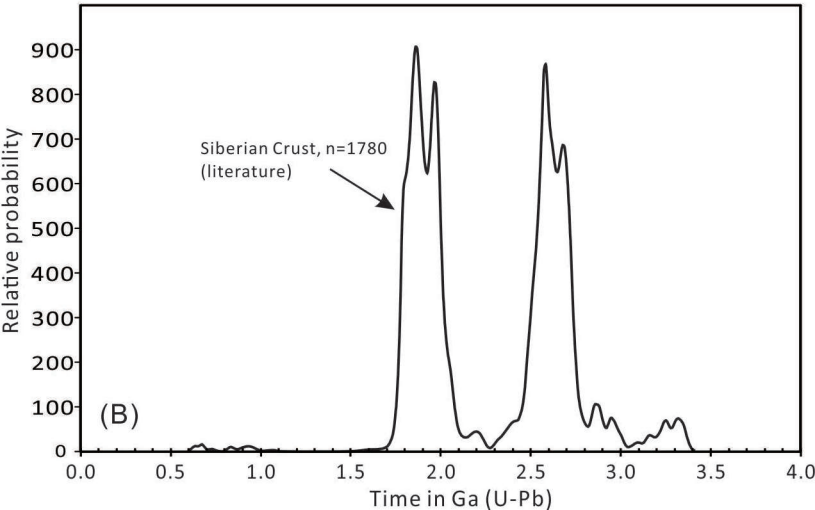
Siberian Crust, n=1780
(literature)
(B)
Relative probability
Time in Ga (U-Pb)

Table 1. Summary of petrologic data for samples in this study

Sample	WR	P	T	WR composition, wt.%			Mg#	Cr#	Modal composition					
number	g	GPa	°C	Al_2O_3	CaO	Mg#	Ol	Spl	Ol	Opx	Cpx	Gar	Spl	Ilm
Olivine megacrysts, and megacrystalline dunite Uv83-13														
U220	93	6.5	1154[d]	0.68	0.47	0.925	0.927	0.90	93	2.3	-	4.2	0.04	-
Uv95-03	71	-	-	0.34	0.21	0.929	0.928	0.86	98	-	-	1.7	0.03	-
Uv83-13	34	-	-	0.55	0.20	0.931	0.933	-	97	-	-	3.0	-	-
Uv569-13	32	4.9	1000[c]	0.22	0.25	0.925	0.926	-	98	0.3	0.9	1.2	-	-
Uv06-17	68	-	-	0.02	0.13	0.929	0.929	0.89	100	0.3	-	-	0.08	-
Averages				*0.36*	*0.25*	*0.928*	*0.929*	*0.88*	*97*	*0.6*		*2.0*		
Coarse dunites														
Uv499-09	93	(4.0)	1028[a]	0.56	0.83	0.922	0.924	0.48	92	3.6	3.5	-	1.0	-
Uv591-09	134	4.0	958[a]	0.23	1.04	0.922	0.923	-	90	5.0	4.4	0.7	-	-
Uv529-10	145	5.4	999[c]	0.66	0.44	0.923	0.926	0.85	91	4.4	0.7	3.7	0.2	-
Uv86-13	145	3.9	946[a]	0.48	0.65	0.924	0.924	-	94	1.6	2.5	2.2	-	-
Uv250-13	71	6.1	1130[d]	1.03	0.28	0.929	0.931	-	93	1.5	-	5.7	-	-
Uv308-13	144	5.2	996[d]	0.74	0.51	0.928	0.934	0.89	94	0.5	-	4.9	0.2	-
Uv571-13	16	-	-	0.31	0.62	0.917	0.932	-	95	-	-	1.6	-	3.2
Uv575-13	63	4.6	783[c]	0.82	0.36	0.926	0.929	-	93	2.1	-	4.5	-	-
Uv85-14	116	(4.0)	857[c]	0.27	0.31	0.930	0.933	0.64	91	8.6	-	-	0.6	-
Averages				*0.57*	*0.56*	*0.925*	*0.928*	*0.71*	*93*	*3.0*	*1.2*	*2.6*		
Sheared dunite														
Uv48-12	44	-	-	0.09	0.48	0.869	0.867	-	99	-	0.5	-	-	-
Low-opx harzburgites														
Uv542-09	142	(3.5)	842[c]	0.9	0.3	0.934	0.934	0.30	83	16	-	-	0.8	-
Uv615-09	77	3.7	857[d]	1.13	1.10	0.925	0.927	0.78	76	18	-	5.4	0.3	0.2
Uv565-10	247	4.2	986[a]	0.84	0.50	0.918	0.921	-	83	13	0.7	3.8	-	-
Uv586-10	124	(3.5)	918[c]	0.25	0.55	0.920	0.920	0.71	78	19	2.0	-	0.3	-
Uv149-11	78	(3.5)	893[c]	0.51	0.52	0.928	0.928	0.56	77	21	1.8	-	0.6	-
Uv44-12	147	(3.5)	977[a]	1.03	0.57	0.922	0.925	0.67	82	12	1.5	3.6	0.5	-
Uv03-13	177	(3.5)	947[c]	0.52	0.35	0.924	0.924	0.47	87	11	1.2	-	0.9	-
Uv63-13	195	5.1	975[d]	0.7	0.8	0.922	0.922	-	85	11	-	4.0	-	-
Uv519-13	215	(3.5)	943[a]	0.82	0.87	0.923	0.929	0.40	82	14	3.5	-	1.0	-
Averages				*0.74*	*0.62*	*0.924*	*0.926*	*0.56*	*81*	*15*	*1.2*	*1.9*	*0.49*	
Opx-rich harzburgites														
Uv101-11	109	(3.5)	961[b]	1.89	0.91	0.929	0.928	0.28	52	46	1.9	-	0.3	-
Uv76-13	223	(3.5)	903[c]	1.19	0.42	0.934	0.933	0.52	55	44	-	-	1.2	-
Averages				*1.54*	*0.66*	*0.931*	*0.931*	*0.40*	*53*	*45*			*0.8*	
Olivine orthopyroxenite														
Uv194-13	120	(2.5)	798[c]	1.82	0.64	0.931	0.931	0.54	21	77	-	-	1.2	-

WR, whole rock (the mass of xenolith material crushed to obtain WR samples is provided). Modal compositions are given normalized to 100% (see text). Ol, olivine; Opx, orthopyroxene; Cpx, clinopyroxene; Gar, garnet; Spl, spinel; Ilm, ilmenite; P, pressure (GPa); T, temperature (°C). Pressure estimated with Opx-Gar method of *Nickel and Green (1985);* values for garnet-free rocks (in parentheses) estimated using P values for samples with similar T's (3.5 or 4.0 GPa). Mineral pairs and methods used for temperature estimates: (a) Cpx-Opx (Taylor, 1998); (b) Ca-in-Cpx (Nimis and Taylor, 2000); (c) Ca-in-Opx (Brey and Kohler, 1990) corrected as in Nimis and Grutter (2010); (d) Opx-Gar (Nimis and Grutter, 2010).

Table 2. Abundances of PGE and Re, $^{187}Re/^{188}Os$ and $^{187}Os/^{188}Os$ ratios, and model age estimates.

N°S	Mg#	Al_2O_3	Os	Ir	Ru	Pt	Pd	Re	$^{187}Re/$	$^{187}Os/$	$^{187}Os/^{188}Os$	$^{PM}T_{RD}$	$^{PM}T_{MA}$	$^{ch}T_{RD}$	$^{ch}T_{MA}$
	wr	wr, %	ppb	ppb	ppb	ppb	ppb	ppb	$/^{188}Os$	$/^{188}Os$	0.36 Ga	Ga	Ga	Ga	Ga
Olivine megacrysts and megacrystalline dunite															
U220	0.925	0.68	7.9	5.0	11.1	7.9	5.6	0.22	0.133	0.11252	0.11172	2.4	3.3	2.3	3.2
Uv95-03	0.929	0.34	6.9	7.6	11.3	6.3	1.3	0.03	0.019	0.10734	0.10723	3.0	3.1	2.9	3.0
Uv83-13	0.931	0.55	3.5	3.6	11.1	2.3	2.1	0.05	0.074	0.11067	0.11023	2.6	3.1	2.5	3.0
Uv569-13	0.925	0.22	15.8	5.0	10.0	9.5	5.0	0.24	0.074	0.11083	0.11038	2.6	3.0	2.5	2.9
Uv06-17	0.929	0.02	7.6	6.1	16.9	7.9	6.6	0.14	0.090	0.11118	0.11064	2.6	3.1	2.5	3.0
Averages	*0.928*	*0.36*	*8.3*	*5.5*	*12.1*	*6.8*	*4.1*	*0.14*				*2.6*	*3.1*	*2.5*	*3.0*
Coarse dunites															
Uv499-09	0.922	0.56	8.6	3.8	7.3	2.5	2.2	0.07	0.038	0.11113	0.11090	2.5	2.7	2.4	2.6
Uv591-09*	0.922	0.23	0.4	7.6	11.0	0.3	0.3	0.30	3.815	0.13489	0.11194	(2.4)	0.1	(2.3)	
Uv529-10	0.923	0.66	1.8	2.4	1.5	0.8	0.3	0.02	0.054	0.11007	0.10975	2.7	3.0	2.6	2.9
Uv86-13*	0.924	0.48	2.2	2.2	9.8	0.9	0.6	0.35	0.749	0.11461	0.11010	(2.6)		(2.5)	
Uv250-13	0.929	1.03	6.3	5.0	4.6	2.4	0.9	0.07	0.054	0.10663	0.10630	3.1	3.5	3.0	3.4
Uv308-13	0.928	0.74	5.0	3.0	9.5	1.9	2.2	0.04	0.039	0.10727	0.10704	3.0	3.3	2.9	3.2
Uv571-13	0.917	0.31	5.9	n.d.	n.d.	n.d.	n.d.	0.07	0.056	0.10752	0.10719	3.0	3.4	2.9	3.3
Uv575-13	0.926	0.82	3.5	14.4	15.8	13.0	7.7	0.05	0.071	0.10912	0.10869	2.8	3.3	2.7	3.2
Uv85-14**	0.930	0.27	4.3	3.0	8.6	2.0	2.6	0.22	0.244	0.12758	0.12611	(0.5)	0.6	(0.5)	
Averages	*0.925*	*0.57*	*4.2*	*5.2*	*8.5*	*3.0*	*2.1*	*0.13*				*2.8*	*3.2*	*2.8*	*3.1*
Sheared dunite															
*Uv48-12**	0.869	0.09	*0.02*	*0.03*	*0.27*	*0.25*	*0.30*	*0.15*	*40.7*	*0.4398*	*0.19480*				
Low-opx harzburgites															
Uv542-09	0.934	0.92	4.0	4.0	5.6	0.3	0.3	0.02	0.024	0.11457	0.11443	2.1	2.2	1.9	2.0
Uv615-09*	0.925	1.13	3.7	3.9	7.2	0.9	0.4	0.68	0.879	0.11739	0.11211	(2.4)		(2.2)	
Uv565-10	0.918	0.84	3.3	3.7	11.6	2.0	2.7	0.02	0.025	0.11553	0.11539	1.9	2.0	1.8	1.9
Uv586-10	0.920	0.25	4.3	9.7	14.5	10.4	0.8	0.11	0.126	0.11556	0.11480	2.0	2.7	1.9	2.5
Uv149-11*	0.928	0.51	3.6	3.9	12.2	1.5	2.1	0.39	0.527	0.12149	0.11832	(1.5)		(1.3)	
*Uv44-12**	*0.922*	*1.03*	*0.03*	*0.21*	*0.55*	*0.15*	*0.25*	*0.01*	*1.22*	*0.12423*	*0.11690*	(1.7)		*(1.5)*	
Uv03-13	0.869	0.09	2.7	2.7	0.9	1.0	0.5	0.02	0.044	0.11565	0.11539	1.9	2.1	1.8	2.0
Uv63-13*	0.922	0.68	0.7	1.2	0.2	0.2	0.4	0.68	4.75	0.14219	0.11359	(2.2)	0.2	(2.0)	
Uv519-13	0.923	0.82	7.5	4.2	12.4	0.1	0.3	0.08	0.053	0.11446	0.11414	2.1	2.3	2.0	2.2
Averages	*0.918*	*0.70*	*3.7*	*3.7*	*7.2*	*1.8*	*0.9*	*0.22*				*2.0*	*2.3*	*1.9*	*2.1*
Opx-rich harzburgites															
*Uv101-11**	*0.929*	*1.89*	*0.04*	*0.34*	*2.24*	*0.14*	*0.46*	*0.01*	*1.305*	*0.12295*	*0.11510*	2.0		*(2.0)*	
*Uv76-13**	*0.934*	*1.19*	*0.01*	*0.03*	*2.08*	*0.09*	*0.30*	*0.04*	*23.66*	*0.2600*	*0.11764*	1.6	0.3	*(1.6)*	
Olivine orthopyroxenite															
Uv194-13	0.931	1.82	2.3	4.8	25.4	39.7	2.5	0.08	0.168	0.12865	0.12764				

$^{187}Os/^{188}Os$ (0.36 Ga) values are recalculated to the eruption age of the host kimberlite (0.36 Ga) using the ^{187}Re decay constant ($\lambda^{187}Re$) of $1.666 \pm 0.005 \times 10^{-11}$ a^{-1} (Smoliar et al. 1996).

$^{PM}T_{RD}$ and $^{PM}T_{MA}$ calculated with PM estimates after Meisel et al. (2001): $^{187}Os/^{188}Os = 0.1296$ and $^{187}Re/^{188}Os = 0.4353$. n.d., not determined;

$^{ch}T_{RD}$ and $^{ch}T_{MA}$ calculated with averages for ordinary and enstatite chondrites (Walker et al., 2002): $^{187}Os/^{188}Os = 0.1282$, $^{187}Re/^{188}Os = 0.4215$.

*Age estimates in parentheses are uncertain due to low Os (≤0.4 ppb) and/or high Re/Os linked to metasomatism before or during eruption.

**Dunite 85-14 has too high $^{187}Os/^{188}Os$ for an ancient melting residue, likely due to later Re enrichment; its T_{RD} and T_{AM} are not meaningful.

Average values for $^{187}Os/^{188}Os$ (0.36 Ga), T_{RD} and T_{MA} disregard samples with low Os and/or high Re/Os, hence uncertain age estimates.

Negative T_{MA} are not shown, they are due to unreasonably high Re/Os in the samples